Biointerface Research in Applied Chemistry
Open-Access Journal (ISSN: 2069-5837)

*Article*
**Volume 16, Issue 3, 2026, 76**
https://doi.org/10.33263/BRIAC163.076

# Exploring FDA-Approved Drugs Against HER2$^+$ Breast Cancer: A Comprehensive *In-Silico* Identification of Lurtotecan as a Promising Candidate

**S.M. Istiaque Hamim [1], Abdul Rashid Issahaku [2], Nor Adila Mhd Omar [1], Kazi Sneha Chhando [1], Sowmitro Das [3], Anke Wilhelm [2], Jufrizal Syahri [4], Roney Miah [1,5,*], Mohd Fadhlizil Fasihi Mohd Aluwi [1,5,*]**

1 Faculty of Industrial Sciences and Technology, Universiti Malaysia Pahang, Al-Sultan Abdullah, Lebuhraya Persiaran Tun Khalil Yaakob, Gambang, Kuantan, Pahang, 26300 Malaysia
2 Department of Chemistry, University of the Free State, 205 Nelson Mandela Avenue, Bloemfontein, 9301 South Africa
3 Laboratory of Pharmaceutical Biotechnology and Bioinformatics, Department of Genetic Engineering and Biotechnology, Jashore University of Science and Technology, Jashore 7408, Bangladesh
4 Department of Chemistry, Universitas Muhammadiyah Riau, Jalan Tuanku Tambusai Ujung, Pekanbaru, Indonesia
5 Centre for Bio-aromatic Research, Universiti Malaysia Pahang Al-Sultan Abdullah, Lebuhraya Persiaran Tun Khalil Yaakob, Gambang, Kuantan, Pahang, 26300 Malaysia
* Correspondence: psk22001@adab.umpsa.edu.my (R.M.); fasihi@umpsa.edu.my (M.F.F.M.A.);
**Received: 10.02.2026; Accepted: 16.05.2026; Published: 15.06.2026**

**Abstract:** HER2 (human epidermal growth factor receptor 2) is a critical oncogenic driver in aggressive breast cancers (BC) and remains an important target for therapeutic intervention. Although targeted therapies such as trastuzumab deruxtecan have shown remarkable efficacy, identifying alternative HER2 inhibitors is essential to overcome resistance and expand treatment options. In this study, an integrated *in-silico* drug repurposing strategy combining pharmacophore-based virtual screening of the DrugBank database, molecular docking, prime Molecular Mechanics Generalized Born Surface Area (MM/GBSA), molecular dynamics (MD) simulations, and post-MD MM/GBSA free energy calculations was applied to identify FDA-approved compounds with potential HER2+ inhibitory activity. The SwissSimilarity screening of the DrugBank database using the pharmacophore-based screening method retrieved fourteen (14) compounds structurally similar to trastuzumab deruxtecan, with similarity scores between 0.352 and 0.751. Further, molecular docking performed using PyRx revealed strong binding affinities ranging from -7.9 to -11.6 kcal/mol, identifying Exatecan (-11.6 kcal/mol), Gimatecan (-10.9 kcal/mol), and Lurtotecan (-10.6 kcal/mol) as top candidates. The clinically approved HER2-targeted drug Trastuzumab Deruxtecan was used as a reference compound for benchmarking the binding interactions, exhibiting a binding affinity of -9.9 kcal/mol. Moreover, prime MM/GBSA calculations supported these findings, with binding free energies of -53.00 kcal/mol for trastuzumab deruxtecan and -45.84 kcal/mol for lurtotecan. MD simulations over 200 ns confirmed the conformational stability of the Lurtotecan-HER2 complex, demonstrating consistent root-mean-square deviation (RMSD) and root-mean-square fluctuations (RMSF) profiles, a stable radius of gyration (RoG), and hydrogen bonding (HB), indicating enhanced structural compactness. Post-MD simulation MM/GBSA analysis revealed a binding free energy of -26.13 ± 8.50 kcal/mol for Lurtotecan, which was comparable to -24.18 ± 6.21 kcal/mol for Trastuzumab Deruxtecan, indicating stable interactions with HER2. Functional enrichment analysis (GO and KEGG) revealed a significant association with oncogenic pathways such as “Pathways in cancer” (hsa05200), involving HER2, PIK3CA, and MTOR. Collectively, these integrative computational findings highlight lurtotecan as a promising candidate for repurposing against HER2$^+$ BC and merit further *in vitro* and *in vivo* evaluation.

**Keywords:** HER2$^+$; breast cancer; drug repurposing; *in-silico*; molecular docking; MD simulations.



## 1. Introduction

Cancer remains a formidable global health concern, significantly affecting individuals, families, and healthcare infrastructures worldwide [1]. The global burden of cancer has steadily increased, with incidence rates rising sharply over the past decade. Data from the International Agency for Research on Cancer (IARC) indicate that cancer cases worldwide increased from 14.1 million in 2012 to nearly 20 million by 2022 [1]. Among the various cancers, breast cancer (BC) ranks as one of the most prevalent and lethal, particularly among women, with an estimated 2.26 million new cases and 685,000 deaths reported in 2020 [2]. Despite significant advances in chemotherapy and targeted therapies, the long-term success of current treatments is often hampered by adverse side effects, acquired drug resistance, and high treatment costs [3]. These challenges highlight the pressing need for novel therapeutic strategies that are both effective and safe, particularly in aggressive subtypes of BC such as those driven by HER2 (human epidermal growth factor receptor 2). HER2, a critical member of the EGFR family, regulates key cellular processes, including proliferation, survival, and apoptosis evasion. Aberrant overexpression or dysregulation of HER2 drives oncogenesis, tumor progression, and increased aggressiveness in approximately 15–20% of BC, often correlating with poor prognosis [4,5].

Current HER2-targeted therapies, including monoclonal antibodies such as Trastuzumab and tyrosine kinase inhibitors such as Lapatinib, have revolutionized treatment paradigms but remain constrained by limited efficacy, resistance development, and toxicity [4]. More recent advancements, such as antibody-drug conjugates (ADCs), including trastuzumab deruxtecan, have demonstrated enhanced selectivity and clinical benefits, even in patients with HER2-low-expressing tumors [6,7]. These therapies leverage targeted delivery of cytotoxic agents to tumor cells, minimizing systemic side effects while improving therapeutic outcomes [8]. Nevertheless, significant challenges persist, including treatment-induced interstitial lung disease, resistance mechanisms, and prohibitive costs, which collectively limit the broad applicability and long-term effectiveness of these agents [9]. The evaluation of these therapies in the literature reveals both their promise and shortcomings: while targeted approaches improve specificity and patient outcomes, they often require combination therapies and intensive monitoring, underscoring the need for alternative, cost-effective, and safe HER2-targeted strategies.

Drug repurposing has emerged as a compelling approach to address these limitations, enabling the identification of new uses for existing, clinically approved compounds and thereby reducing development time, costs, and safety risks [10]. Computational strategies have further strengthened this paradigm, particularly ligand-based virtual screening methods. Tools like SwissSimilarity enable rapid identification of compounds structurally similar to known therapeutics, facilitating the discovery of novel candidates with potential HER2-targeting activity [11,12]. In the present study, trastuzumab deruxtecan was selected as the reference pharmacophore template because it represents a clinically validated HER2-targeted therapeutic agent with demonstrated efficacy against HER2$^+$ and HER2-low BCs, making it a relevant

structural benchmark for identifying compounds that may share similar interaction features with the HER2 receptor [6,13]. While virtual screening accelerates drug discovery and expands the pool of candidate molecules, its predictive accuracy can be limited by the quality of the input data and scoring algorithms, often necessitating complementary validation techniques [14]. In addition, molecular docking and binding free energy calculations, such as Prime MM/GBSA, provide quantitative estimates of ligand-receptor affinities and interaction profiles [15]. These methods, however, typically assume rigid receptor conformations and may overlook dynamic behaviors that are critical for accurate predictions. Molecular dynamics (MD) simulations and post-MD MM/GBSA can address these limitations by modeling protein-ligand interactions over time and providing insights into conformational stability, though they are computationally intensive [16,17]. It is important to note that *in silico* predictions, while valuable for prioritizing candidates, cannot fully capture complex cellular contexts, pharmacokinetics, or off-target effects and therefore require subsequent experimental validation to confirm therapeutic relevance.

It is important to note that in-silico predictions, while valuable for prioritizing candidate molecules, cannot fully capture complex cellular environments, pharmacokinetics, or potential off-target effects. Therefore, computational findings should be interpreted cautiously and considered as hypothesis-generating tools that require subsequent experimental validation to confirm their therapeutic relevance [14,16].

In addition to structure-based approaches, network pharmacology (NP) analyses were conducted to elucidate its mechanism of action against $HER2^+$ BC. Studies show that integrating computational approaches such as virtual screening, docking, MM/GBSA, MD simulations, and NP provides a balanced strategy. By combining these methods, researchers can leverage their individual strengths while mitigating their limitations, ultimately increasing confidence in selecting promising candidates.

In this study, we applied a multi-tiered *in silico* strategy to identify potential HER2-targeting agents via drug repurposing. The DrugBank database was screened using a pharmacophore-based approach implemented in SwissSimilarity, with trastuzumab deruxtecan serving as the reference compound to identify FDA-approved drugs with structural and functional similarity. A pharmacophore-based approach was employed to screen DrugBank compounds, based on the hypothesis that molecules with similar pharmacophore features may exhibit comparable activity, enabling the identification of potential alternative therapies for $HER2^+$ BC. Promising candidates were then subjected to molecular docking and Prime MM/GBSA calculations to evaluate their binding affinities and interaction profiles. To further investigate the dynamic stability of the protein-ligand complexes, MD simulations were followed by post-MD MM/GBSA analyses. Among the compounds examined, Lurtotecan, a topoisomerase I inhibitor previously tested in clinical trials for ovarian and lung cancers, demonstrated strong and stable interactions within the HER2 active site [18,19]. Although Lurtotecan is primarily known as a topoisomerase I inhibitor [20], recent computational and multi-target pharmacology studies suggest that certain anticancer agents may interact with multiple molecular targets, raising the possibility that such compounds could also engage alternative cancer-related proteins, including receptor tyrosine kinases such as HER2 [21,22]. Additionally, NP analyses were conducted to elucidate its potential mechanisms of action against $HER2^+$ BC. This integrated computational workflow not only identifies promising repurposed candidates but also provides detailed insights into their interaction patterns and

mechanistic pathways, establishing a rational basis for future experimental validation and the development of safer, more effective HER2-targeted therapies.

## 2. Materials and Methods

### *2.1. Ligand selection.*

The SMILES notation for Trastuzumab Deruxtecan was retrieved from the DrugBank database (https://go.drugbank.com/) and utilized as input for compound similarity analysis using the SwissSimilarity platform (http://www.swisssimilarity.ch/), an online tool designed for virtual screening based on molecular features [12]. Through the pharmacophore-based screening mode, structurally related FDA-approved compounds were identified within the DrugBank library. The shortlisted ligands were subsequently downloaded from the PubChem database (https://pubchem.ncbi.nlm.nih.gov/) for further computational analyses.

### *2.2. Active site prediction.*

The identification of the protein active site is an important step in structure-based drug design, as ligand binding within this region is crucial for regulating protein function and ensuring stable ligand-protein interactions [23]. In this study, the active binding site of the target protein was determined using the PyMOL Visualizer Tool (version 3.1.1) through structural inspection of the protein structure [23]. The predicted binding pocket includes the residues LEU726, VAL734, ILE752, LYS753, ALA771, MET774, ARG784, LEU785, LEU796, VAL797, THR798, GLN799, LEU800, MET801, CYS805, LEU807, ASP808, ARG849, LEU852, THR862, and PHE864, which were selected as the docking region for subsequent molecular docking analysis.

### *2.3. Molecular docking and prime MM/GBSA.*

Molecular docking studies were performed to evaluate the binding affinity and interaction modes of selected ligands with the HER2 receptor using PyRx (version 0.8), which employs AutoDock Vina as the docking engine [24,25]. The three-dimensional crystal structure of HER2 was retrieved from the Protein Data Bank with PDB ID: 7PCD. Protein preparation steps, including removal of water molecules, heteroatoms, and co-crystallized ligands, were carried out using Discovery Studio Visualizer [26]. Hydrogen atoms were added, and Gasteiger charges were assigned using AutoDock Tools [27].

Ligands were downloaded in SDF format from the PubChem and converted into minimized structures using the Open Babel plugin in PyRx with the Universal Force Field (UFF) [28]. The docking grid box was defined to cover the HER2 binding pocket with the center coordinates set at X: 6.8146, Y: -8.1710, Z: -13.2531, and grid box dimensions of 30.7632 × 33.9697 × 31.1758 Å along the X, Y, and Z axes, respectively. Docking simulations were performed using AutoDock Vina with an exhaustiveness parameter of 8, after converting the receptor and ligands into PDBQT format [29,30]. The resulting binding affinities (kcal/mol) and docking conformations were analyzed, and the best pose for each ligand was selected based on the lowest binding energy and appropriate orientation within the binding pocket. Key molecular interactions, including hydrogen bonds, π–π stacking, halogen interactions, and hydrophobic contacts, were visualized and interpreted using Discovery Studio Visualizer.

To further refine the docking results, the binding free energies of the HER2-ligand complexes were estimated using the Prime Molecular Mechanics Generalized Born Surface Area (MM/GBSA) method implemented in the Schrödinger Suite (version 2019-2) [31]. The binding free energy ($\Delta G_{bind}$) was calculated according to the equation:

$$\Delta G_{bind} = \Delta E_{MM} + \Delta G_{solv} + \Delta G_{SA} \quad (1)$$

Where, $\Delta E_{MM}$ represents the molecular mechanics energy, encompassing bonded, van der Waals, and electrostatic interactions. The solvation energy ($\Delta G_{solv}$) was calculated using the VSGB implicit solvent model to capture polar interactions, while the surface area term ($\Delta G_{SA}$) accounts for nonpolar solvation energy based on the solvent-accessible surface area (SASA). All calculations were performed using the OPLS force field. MM/GBSA analysis was conducted on the minimized docking complexes obtained from the docking results to estimate the binding free energy of each ligand-HER2 complex. It should be noted that the entropy contribution to binding free energy was not calculated due to the high computational cost and the complexity of obtaining reliable estimates, which represents a limitation of this study.

*2.4. Molecular dynamics (MD) simulations.*

To assess the structural stability, flexibility, and dynamic behavior of the HER2-ligand complexes, MD simulations were carried out using the AMBER18 software suite [32]. The ff14SB force field was applied to the protein, while ligand topologies were prepared using the GAFF (General AMBER Force Field) with AM1-BCC charges generated via the Antechamber module [33]. Topology and coordinate files were built using tleap, and each complex was solvated in an octahedral box of TIP3P water molecules with a 10 Å buffer and neutralized by adding counterions [34]. The systems were first minimized in two steps: a restrained minimization of the solute, followed by minimization of the entire system. Equilibration involved gradual heating from 0 K to 300 K under the NVT ensemble for 100 ps, followed by 500 ps under NPT conditions at 1 atm [35–37]. Temperature and pressure were controlled using the Langevin thermostat and Berendsen barostat, and protein backbone restraints were progressively relaxed. Production runs were performed for 250 ns under constant pressure and temperature (NPT ensemble) with a 2-fs time step, employing the SHAKE algorithm to constrain hydrogen-involved bonds and the Particle Mesh Ewald (PME) method for long-range electrostatics (10 Å cutoff) [38–40]. Trajectories were saved every 10 ps and analyzed using CPPTRAJ [41], which provided key metrics including Root Mean Square Deviation (RMSD), Root Mean Square Fluctuation (RMSF), Radius of Gyration (RoG), and the number of intramolecular hydrogen bonds (HBs), thereby offering detailed insight into the stability and conformational dynamics of the HER2-ligand systems over time.

*2.5. Principal component analysis (PCA) and free-energy landscape (FEL).*

To investigate the essential dynamics and conformational behavior of the HER2–ligand complexes, Principal Component Analysis (PCA) and Free Energy Landscape (FEL) analyses were performed using the AMBER18 [42]. The 250 ns MD simulation trajectories were processed using the cpptraj module. Solvent molecules and counterions (WAT, $Na^+$, $Cl^-$) were removed using the strip command, and structural alignment was performed with rms first to eliminate translational and rotational motions. PCA was conducted by calculating the mass-weighted covariance matrix of the backbone atomic positional fluctuations (matrix covar name

covar out covar.dat), which was diagonalized using analyze matrix covar out evecs.dat vecs 20 to obtain the top 20 eigenvectors representing collective motions. The first two principal components (PC1 and PC2), representing the most significant large-scale motions, were selected for analysis, and the percentage of total variance explained by PC1 and PC2 was calculated and reported to quantify their contribution to overall protein motion [43]. Trajectory projections along these components were generated using the projection command.

For FEL construction, the projection data of PC1 and PC2 were used to map the conformational landscape of the protein–ligand systems. The free energy at each point on the 2D plot was calculated using the Boltzmann relation:

$$G(x, y) = -kBT \ln P(x, y) \quad (2)$$

where P(x,y)P(x, y)P(x,y) is the probability density of the system at the corresponding principal component coordinates, kBk_BkB is the Boltzmann constant, and TTT is the absolute temperature. These values were binned and plotted using visualization tools such as GNUplot or Origin, with lower energy regions indicating more stable conformational states. The FEL plots revealed the distribution of energy minima and the most frequently sampled conformations, providing insight into the thermodynamic stability and flexibility of the HER2–ligand complexes throughout the simulation.

*2.6. Binding free energy calculation using MM/GBSA.*

The binding free energy (ΔGbind) of the HER2-ligand complexes was calculated using the Molecular Mechanics/Generalized Born Surface Area (MM/GBSA) approach implemented in the AMBER18 software package [41]. Post-processing of the 250 ns MD trajectories was performed using the MMPBSA.py module [44]. Representative snapshots were extracted at regular intervals from the last 100 ns of the MD trajectory to ensure equilibrium sampling. The MM/GBSA method estimates the binding free energy as the difference between the free energy of the complex and the sum of the free energies of the unbound receptor and ligand, calculated using the formula:

$$\Delta G_{bind} = G_{complex} - (G_{protein} + G_{ligand}) \quad (3)$$

The total binding free energy includes contributions from van der Waals energy ($\Delta E_{vdW}$), electrostatic energy ($\Delta E_{ele}$), polar solvation energy ($\Delta G_{polar}$), and nonpolar solvation energy ($\Delta G_{nonpolar}$). The gas-phase energy ($\Delta G_{gas}$) is the sum of van der Waals and electrostatic energies, while the solvation energy ($\Delta G_{sol}$) is the sum of polar and nonpolar solvation components. The calculations were carried out with the generalized Born (GB) implicit solvent model (igb=5), and a salt concentration of 0.150 M was set to mimic physiological conditions. The results provided insights into the thermodynamic favorability and strength of interactions between HER2 and the bound ligands, supporting conclusions drawn from molecular docking and MD simulations.

*2.7. Mechanism of action study.*

2.7.1. Network construction, gene ontology (GO), and Kyoto Encyclopedia of genes and genomes (KEGG) pathway enrichment analysis.

The Simplified Molecular Input Line Entry System (SMILES) representations of the selected compounds were obtained from the DrugBank. Potential targets associated with $HER2^+$ BC were retrieved from GeneCards by searching the keyword "$HER2^+$ Breast Cancer in Human" [45]. To predict the protein targets of Lurtotecan, the SwissTargetPrediction was employed [46]. Overlapping targets between Lurtotecan and $HER2^+$ BC were identified using Venny 2.1.0 [47]. A compound-target interaction network was constructed using STRING [48], applying a high confidence threshold of 0.7 to include only robust protein–protein interactions, and the network was visualized with Cytoscape version 3.10.2 [49].

Functional enrichment analyses were then performed to explore the potential mechanisms of Lurtotecan against $HER2^+$ BC. Gene Ontology (GO) annotation and Kyoto Encyclopedia of genes and genomes (KEGG) pathway mapping were conducted using the DAVID platform [50], and results were visualized using the Micro-Informatics online tool (https://www.bioinformatics.com.cn/). GO terms were classified into Biological Processes (BP), Cellular Components (CC), and Molecular Functions (MF). To ensure statistical rigor, enrichment analyses were filtered using a p-value $< 0.05$ and adjusted for multiple testing using the Benjamini–Hochberg (FDR) correction, controlling for false discovery. KEGG pathway analysis was performed on the overlapping gene set of Lurtotecan and $HER2^+$ BC to identify key signaling pathways potentially mediating therapeutic effects.

## 3. Results and Discussion

### *3.1. Ligand selection.*

Using pharmacophore-based virtual screening on the SwissSimilarity platform, 14 compounds exhibiting structural similarity to trastuzumab deruxtecan were identified. The selected ligands displayed similarity scores ranging from 0.352 to 0.751, reflecting diverse levels of structural resemblance. Table 1 presents an overview of these compounds, including their DrugBank identifiers and corresponding similarity scores.

### *3.2. Molecular docking and prime MM/GBSA.*

Molecular docking is a key computational technique in drug discovery that predicts and evaluates how ligands interact with target proteins at the molecular level, enabling the identification and selection of compounds with high potential for further development, such as those showing favorable binding energies and interactions with the HER2 receptor, whose overexpression in BC is associated with aggressive tumor progression and poor clinical outcomes [5,51–53]. This in silico technique enables researchers to predict binding affinity and molecular interactions between potential drug candidates and the HER2 receptor, thereby accelerating the identification and optimization of novel inhibitors [52,53]. By virtually screening extensive chemical libraries, molecular docking efficiently prioritizes compounds with strong binding potential, thereby significantly reducing the need for labor-intensive, costly experimental assays [53,54]. To complement docking studies, Prime MM/GBSA has emerged as a critical tool in HER2 inhibitor discovery. It serves both as a robust method for estimating binding free energies and as a means to validate docking results [55,56]. This approach combines Prime's high-accuracy energy minimization with the MM/GBSA algorithm to provide detailed, quantitative insights into the binding affinities between HER2 and candidate inhibitors [55,57]. By analyzing snapshots from MD simulations, Prime MM/GBSA provides a more reliable estimate of binding free energy than docking scores alone, often yielding better

correlation with experimental data [57]. Moreover, it is widely employed to rescore docking poses, helping to ensure that predicted ligand conformations are energetically stable and favorably positioned within the HER2 binding pocket, thereby increasing confidence in virtual screening outcomes [56,57].

Based on the molecular docking and Prime MM/GBSA results illustrated in Figure 1 and summarized in Table 1, various camptothecin derivatives and other anticancer agents demonstrated notable binding affinities toward the target protein, as indicated by both molecular docking scores and Prime MM/GBSA binding free energies. Among the tested compounds, TAK-733 showed the most favorable Prime MM/GBSA binding free energy (-59.46 kcal/mol) despite having the lowest docking score (-7.9 kcal/mol). This compound formed two hydrogen bonds with MET801 and ASN850 and participated in multiple hydrophobic interactions involving LEU852, LEU726, VAL734, ALA751, LYS753, and LEU796, suggesting a stable binding mode through a combination of polar and non-polar interactions. Similarly, RO-4987655 exhibited a highly favorable Prime MM/GBSA energy (-53.53 kcal/mol) with a moderate docking score of -8.9 kcal/mol and formed hydrogen bonds with LYS753 and PHE864.

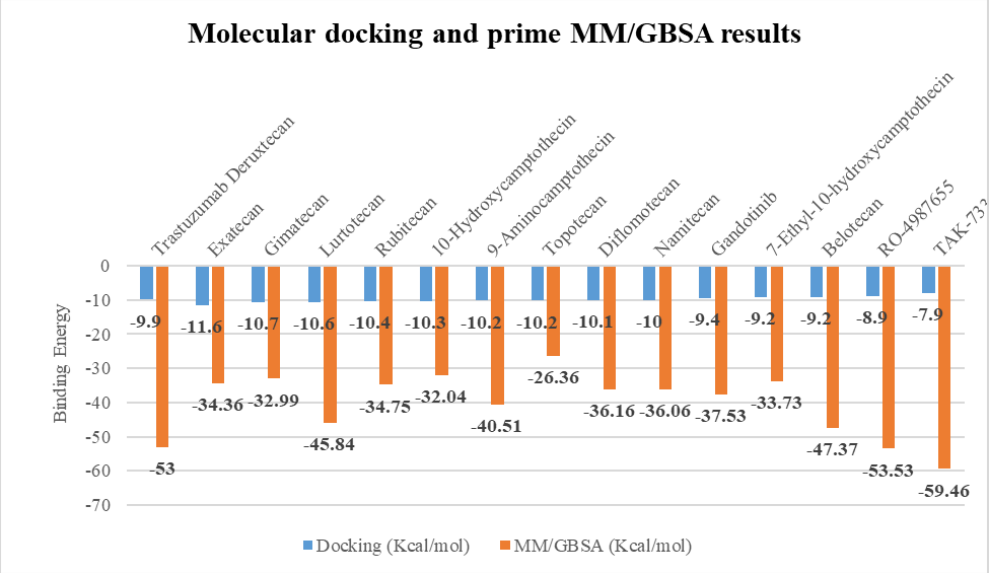


**Figure 1.** Molecular docking and Prime MM/GBSA analysis of Trastuzumab Deruxtecan and 14 analogs, showing their binding energies within the HER2 active site (PDB ID: 7PCD).

**Table 1.** Binding affinities of Trastuzumab Deruxtecan and 14 analogs with HER2 (PDB ID: 7PCD), including docking scores, Prime MM/GBSA-calculated energies, and interactions with amino acid residues in the protein's active site.

| Compound name | Drug bank ID | Similarity score | Molecular docking energy | Prime MM/GBSA (Kcal/mol) | Binding amino acid |
|---|---|---|---|---|---|
| Trastuzumab Deruxtecan (Control) | DB14962 | 1.000 | -9.9 | -53.00 | LYS753, LEU785 (H-B), PHE864 (Halogen-Fluorine), ASP863 (Pi-sigma/ Amide pi-stacked), VAL734, ALA751, ILE767 (pi Alkyl). |
| Exatecan | DB12185 | 0.751 | -11.6 | -34.36 | LYS753, MET801, ASP863 (H-B), VAL734, LEU752 (Pi-Sigma), LEU726, ALA751 (Alkyl/pi-Alkyl). |
| Gimatecan | DB06721 | 0.357 | -10.7 | -32.99 | LYS753, ASP863 (H-B), VAL734, LEU852 (Pi Sigma), LEU726, ALA751, CYS805 (Alkyl/ pi Alkyl). |

| Compound name | Drug bank ID | Similarity score | Molecular docking energy | Prime MM/GBSA (Kcal/mol) | Binding amino acid |
|---|---|---|---|---|---|
| Lurtotecan | DB12222 | 0.448 | -10.6 | -45.84 | LYS753, ASN850, ASP863 (H-B), LEU726, VAL734 (Pi-sigma), ALA751, LEU852 (Alkyl/pi-Alkyl). |
| Rubitecan | DB06159 | 0.391 | -10.4 | -34.75 | LYS753, ASP863 (H-B), LEU724, VAL734, LEU852 (pi-sigma), ALA751, LEU785, LEU796 (Alkyl/pi-Alkyl). |
| 10-Hydroxycamptothecin | DB12385 | 0.435 | -10.3 | -32.04 | LYS753, SER783, THR862, ASP863 (H-B), VAL734, LEU852 (Pi-sigma), LEU726, ALA751 (Pi Alkyl). |
| 9-Aminocamptothecin | DB12515 | 0.381 | -10.2 | -40.51 | LYS753, ASP863 (H-B), LEU726, VAL734, LEU852 (pi-sigma), ALA75 (Pi-Alkyl). |
| Topotecan | DB01030 | 0.434 | -10.2 | -26.36 | LYS753, MET801, ASP863 (H-B), LEU726, VAL734, LEU852 (Pi-sigma), ALA751 (pi-Alkyl) |
| Diflomotecan | DB16138 | 0.409 | -10.1 | -36.16 | CYS805, GLY804 (H-B), VAL734 (Pi sigma), ALA751, LYS753, LEU852 (pi Alkyl). |
| Namitecan | DB12124 | 0.432 | -10.0 | -36.06 | LYS753, ARG849, ASN850, ASP863 (H-B), LEU726, VAL734, LEU852 (pi-sigma), ALA751 (Pi Alkyl). |
| Gandotinib | DB13040 | 0.352 | -9.4 | -37.53 | MET801, ARG849, ASP863 (H-B), LEU726, VAL734, LEU852 (pi-Sigma), ALA751, LYS753, ALA771, LEU785, LEU800 (Alkyl/ Pi-Alkyl). |
| 7-Ethyl-10-hydroxycamptothecin | DB05482 | 0.485 | -9.2 | -33.73 | ILE767, ASP863 (H-B), VAL734 (Pi-sigma), PHE864 (Pi-pi T shaped), ALA751, LYS753, LEU785, LEU796, LEU852 (Alkyl/Pi-Alkyl). |
| Belotecan | DB12459 | 0.394 | -9.2 | -47.37 | ASP863 (H-B), LYS753 (Pi-Cation), VAL734 (Pi-sigma), PHE864 (Pi-pi T-shaped), ALA751, LEU785, LEU852 (Pi-Alkyl). |
| RO-4987655 | DB12933 | 0.355 | -8.9 | -53.53 | LYS753, PHE864 (H-B), VAL734, ALA771, MET774, LEU785 (Alkyl/ Pi-Alkyl). |
| TAK-733 | DB12241 | 0.369 | -7.9 | -59.46 | MET801, ASN850 (H-B), THR798, LEU852 (Pi-sigma), LEU726, VAL734, ALA751, LYS753, LEU796 (Alkyl/Pi-Alkyl) |

Among the camptothecin derivatives, Lurtotecan and Belotecan were notable for their high Prime MM/GBSA values (-45.84 and -47.37 kcal/mol, respectively). Lurtotecan formed three hydrogen bonds (LYS753, ASN850, ASP863) and stabilized within the binding pocket via π - σ and hydrophobic interactions (Figure 2a). Belotecan, although forming only one hydrogen bond (with ASP863), exhibited strong π-cation and alkyl interactions with critical residues like LYS753, VAL734, and LEU852. 10-Hydroxycamptothecin and 9-Aminocamptothecin also showed favorable binding, with docking scores of -10.3 and -10.2

kcal/mol and Prime MM/GBSA energies of -32.04 and -40.51 kcal/mol, respectively. Particularly, 10-Hydroxycamptothecin demonstrated a dense hydrogen bonding network (four H-bonds) with LYS753, SER783, THR862, and ASP863, highlighting its potential stability and binding efficiency within the pocket. Other compounds, such as Gimatecan, Rubitecan, and Exatecan, also showed strong docking scores and interacted consistently with key residues, including LYS753, ASP863, VAL734, and ALA751, reinforcing the significance of these residues in ligand anchoring. The control compound, Trastuzumab Deruxtecan, also showed strong binding energy (-53.00 kcal/mol) with hydrogen bonds and halogen and π-interactions involving key residues such as LYS753, ASP863, PHE864, and ALA751 (Figure 2b).

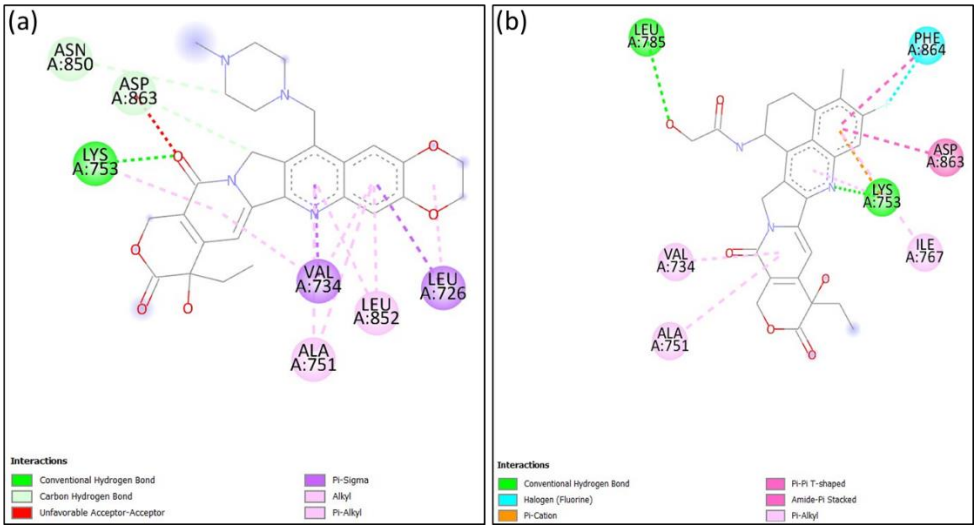


**Figure 2.** Molecular docking interaction analysis of HER2 protein complexes with **(a)** Lurtotecan; **(b)** Trastuzumab Deruxtecan (control), highlighting key amino acid interactions, hydrogen bonds, and binding orientations within the active site.

Compounds such as Namitecan, Topotecan, and Diflomotecan display docking scores in the range of -10.0 to -10.2 kcal/mol and moderate Prime MM/GBSA energies, with Namitecan forming four hydrogen bonds, suggesting potential binding stability. Gandotinib and 7-Ethyl-10-hydroxycamptothecin showed slightly weaker docking scores (-9.4 and -9.2 kcal/mol) but maintained considerable MM/GBSA values and diverse interactions, including π-π T-shaped and hydrophobic contacts.

Notably, docking scores provide a preliminary assessment of binding potential; chemical similarity alone does not guarantee HER2 kinase inhibition. Therefore, our interpretation relies on both binding energies and detailed interaction analysis, including hydrogen bonding, hydrophobic contacts, and π-stacking interactions, which are more predictive of inhibitory potential [58]. Additionally, the unusually high electrostatic term observed for Lurtotecan during MM/GBSA analysis was re-evaluated, and the total binding free energy ($\Delta G_{bind}$) was considered the more reliable indicator of overall binding stability, in line with established computational protocols for MM/GBSA [59,60].

Overall, the docking and MM/GBSA analyses indicate that several camptothecin analogs, particularly Lurtotecan, Belotecan, and 10-Hydroxycamptothecin, exhibit strong binding profiles characterized by significant hydrogen bonding and hydrophobic interactions. Conserved residues such as LYS753, ASP863, VAL734, ALA751, and LEU852 were frequently involved in ligand binding, highlighting their crucial role in stabilizing compound-protein complexes. Lurtotecan has demonstrated notable anticancer properties, primarily through its inhibition of topoisomerase I, an essential enzyme involved in DNA replication in

cancer cells [61]. Molecular docking studies have been pivotal in elucidating the binding mode of Lurtotecan to topoisomerase I, confirming that the drug effectively stabilizes the topoisomerase I-DNA cleavage complex, thereby inducing lethal DNA breaks within proliferating tumor cells [61,62]. These computational approaches enable visualization and quantification of Lurtotecan's interactions at the atomic level, helping researchers predict its binding affinity and optimize its molecular structure to enhance potency and reduce toxicity. In-silico analyses also support the efficient screening of Lurtotecan derivatives and analogs, accelerating the discovery of new lead compounds against various cancer types while minimizing the need for extensive in-vitro experimentation [62]. Thus, molecular docking has proven indispensable for both understanding and advancing the anticancer application of Lurtotecan. These findings suggest the promising therapeutic potential of selected derivatives for further pharmacological development.

*3.2. Molecular dynamics (MD) simulations.*

MD simulations were conducted over a 250 ns timescale to evaluate the structural stability, flexibility, compactness, and HB behavior of the HER2 receptor in three distinct states: unbound (apo), complexed with Lurtotecan, and complexed with reference compound Trastuzumab Deruxtecan. Among the various structural metrics, RMSD serves as a critical parameter for assessing the conformational stability of protein-ligand complexes. RMSD quantifies the average positional deviation of atoms, typically backbone or heavy atoms, relative to a reference structure over time, providing insight into the overall structural integrity of the protein-ligand complex [5,63]. A low and stable RMSD value generally indicates that the complex remains conformationally stable, supporting the hypothesis of strong and specific ligand binding, which is an essential attribute for therapeutic efficacy [5,63]. RMSD analysis revealed that the apo HER2 receptor exhibited the highest average structural deviation (3.01 ± 0.28 Å), indicating notable conformational fluctuations throughout the simulation period (Figure 3a and Table 2). In contrast, the Lurtotecan-HER2 complex demonstrated a substantially lower average RMSD (2.55 ± 0.25 Å), suggesting enhanced structural stability and minimal deviation from its initial conformation (Figure 3a and Table 2). The control complex with Trastuzumab Deruxtecan also maintained considerable structural integrity, with an average RMSD of 2.83 ± 0.35 Å, slightly higher than that of Lurtotecan but still within a stable range (Figure 3a and Table 2). Novel pyrazoline-based HER2 inhibitors exhibited RMSD values of approximately 1.0–2.5 Å over a 200 ns simulation, indicating stable binding within the kinase pocket [64]. Similarly, computational screening of natural compounds against HER2 showed RMSD trajectories of 2-3 Å over 50 ns, reflecting good conformational stability [5].

In contrast, ligand-HER2 complexes with soil-derived bacterial metabolites displayed higher backbone fluctuations, with an average RMSD of 3.4 Å over 100 ns [65]. Although the absolute differences in RMSD values between the complexes are relatively modest, even small reductions in RMSD can reflect meaningful stabilization at the binding site, especially when considered alongside other complementary metrics such as hydrogen bonding, interaction energies, and conformational clustering [66]. These findings suggest that ligand binding, particularly with Lurtotecan, contributes to the conformational stabilization of the HER2 receptor, likely through favorable interactions that restrict structural fluctuations and promote better accommodation of the ligand within the binding pocket.

**Table 2.** RMSD, RMSF, RoG, and HB analyses of the apo HER2 protein, Lurtotecan-HER2 complex, and control-HER2 complex over a 250 ns MD simulation, illustrating structural stability, residue flexibility, compactness, and ligand-induced interactions.

| System | RMSD Å | RMSF Å | RoG Å | HB |
|---|---|---|---|---|
| Apo | 3.01±0.28 | 1.32±0.66 | 19.53±0.21 | 127.78±8.44 |
| Lurtotecan complex | 2.55±.25 | 1.30±1.08 | 19.35±0.11 | 128.18±8.07 |
| Control complex | 2.83±0.35 | 1.09±0.68 | 19.16±0.12 | 132.95±7.98 |

RMSF is a vital parameter that provides residue-level insights into protein flexibility and dynamic behavior during ligand binding. RMSF analysis offers a detailed understanding of how individual amino acid residues fluctuate over time in response to ligand interaction. While RMSD captures global conformational stability, RMSF highlights local fluctuations, identifying flexible regions that may play critical roles in ligand binding, allosteric regulation, or conformational transitions [67]. This information is particularly valuable for rational drug design, as targeting and stabilizing key flexible regions may enhance inhibitor efficacy and binding specificity [68]. RMSF analysis revealed notable differences in residue flexibility across the three simulation systems. The apo HER2 receptor exhibited an average RMSF of 1.32 ± 0.66 Å, with prominent fluctuations observed in the loop and terminal regions (Figure 3b and Table 2). Complexation with Lurtotecan led to a marginal decrease in RMSF (1.30 ± 1.08 Å), indicating a slight reduction in flexibility, particularly in residues located near the binding site (Figure 3b and Table 2). The control complex with Trastuzumab Deruxtecan showed the lowest average RMSF (1.09 ± 0.68 Å), suggesting that the control ligand induces a more rigid, conformationally restrained structure (Figure 3b and Table 2). Notably, regions corresponding to residue indices 60-80 and 250-280 in the apo structure exhibited peak fluctuations, indicative of highly mobile loops (Figure 3b). These fluctuations were markedly dampened in both ligand-bound complexes, implying that ligand engagement restricts the motion of these flexible segments. MD simulations of HER2 with curcumin derivatives showed that ligand binding reduced fluctuations in key residues compared to the unbound protein, indicating stabilization upon complexation [69]. Similarly, complexes with natural compounds ZINC43069427 and ZINC95918662 exhibited low RMSF (0.12 nm) over 50 ns, suggesting rigidification of the binding region [5]. MD studies of the HER2 kinase domain also revealed that flexible loop regions, such as the αC-β4 loop, often become stabilized or redistributed upon ligand binding [70]. This conformational constraint likely contributes to the structural stabilization of the HER2 receptor, further supporting the potential of Lurtotecan as an effective HER2-targeted therapeutic agent.

RoG is a key structural parameter offering insight into the overall compactness and conformational stability of protein-ligand complexes. RoG serves as a valuable metric for assessing how ligand binding influences the receptor's spatial arrangement and folding [71,72]. RoG measures the root-mean-square distance of atoms from the protein's center of mass, with lower, more stable values indicating a compact, coherent structure, important for protein function and inhibitor binding [71,73]. The unbound (apo) HER2 receptor maintained an average RoG of 19.53 ± 0.21 Å, indicating a relatively loose and expanded conformation (Figure 3c and Table 2). Upon ligand binding, a notable decrease in RoG was observed: 19.35 ± 0.11 Å for the Lurtotecan complex and 19.16 ± 0.12 Å for the control complex (Figure 3c and Table 2). Several MD simulation-based studies of HER2 have observed protein RoG values around 1.7-2.0 nm, with either stable or slightly reduced values upon ligand binding, indicating that ligand interactions may compact and stabilize the protein structure [4,5,74]. This reduction suggests that ligand interaction promotes a more compact and tightly folded protein structure.

The greater compactness in the ligand-bound forms also implies reduced solvent-accessible surface area, further supporting the stabilizing influence of both Lurtotecan and the reference compound. These results collectively indicate that ligand binding, particularly with Lurtotecan, contributes to the conformational tightening of the HER2 receptor, enhancing its structural integrity and supporting its potential role as a viable therapeutic candidate.

HB plays a pivotal role, particularly in evaluating the stability and specificity of protein-ligand interactions. The formation and persistence of HBs between receptor and candidate ligands significantly stabilize the complex, enhancing binding affinity and, consequently, therapeutic efficacy [52,54]. In addition to direct ligand interactions, intra-protein HBs are equally important, as they maintain the integrity of the protein's tertiary structure throughout the simulation. The average number of intra-protein HB was highest in the control complex (132.95 ± 7.98), followed by the Lurtotecan-bound HER2 complex (128.18 ± 8.07), and lowest in the apo form (127.78 ± 8.44) (Figure 3d and Table 2). The increased HBs in both ligand-bound complexes, relative to the unbound receptor, suggest that ligand interaction reinforces the structural cohesion of HER2. This stabilization effect is particularly evident with Lurtotecan, which demonstrated a HB profile comparable to that of the reference compound. MD simulation-based studies on HER2 and its binding partners indicate that ligand or antibody engagement reinforces inter- and intra-domain interactions by creating new HBs and modifying existing ones, leading to decreased fluctuations and greater structural stability [70,75]. These findings underscore the role of HBs in mediating the conformational stability of HER2 upon ligand engagement. Lurtotecan's ability to maintain a high number of stabilizing interactions further supports its potential as a promising HER2-targeted therapeutic agent with strong binding affinity and structural compatibility.

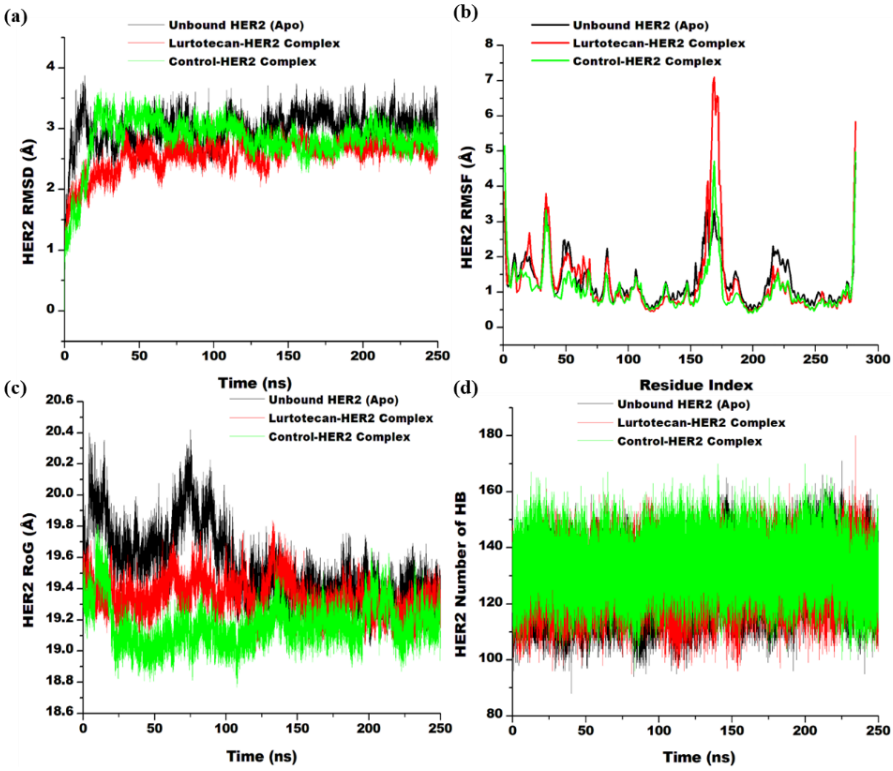


**Figure 3.** Molecular dynamics (MD) simulations analysis of the HER2 protein over 250 ns, showing **(a)** RMSD; **(b)** RMSF; **(c)** RoG; **(d)** hydrogen bond (HB) profiles for the apo protein (black), Lurtotecan-HER2 complex (red), and control-HER2 complex (green), illustrating structural stability, residue flexibility, compactness, and ligand-induced interactions.

*3.3. Principal component analysis (PCA) and free-energy landscape (FEL).*

PCA is a powerful tool that enables the exploration of large-scale conformational motions in biomolecular systems. This study provides critical insights into the dynamic behavior and essential motions of the HER2-ligand complex [76]. By reducing the high-dimensional dataset of atomic displacements into a set of orthogonal principal components (PCs), PCA identifies the dominant motions contributing to the system's overall structural variance. This decomposition enables differentiation between biologically relevant conformational transitions and random thermal fluctuations, thereby revealing how ligand binding shapes the HER2 receptor's conformational landscape and functional states [76,77]. The PCA plot displays the conformational sampling of the HER2 receptor projected onto the first two principal components (PC1 and PC2), comparing three systems: apo HER2 (black), the Lurtotecan-HER2 complex (red), and the Control-HER2 complex (green) (Figure 4a). The unbound HER2 system exhibits broad dispersion along negative PC1 and neutral-to-negative PC2 values, suggesting a wider conformational space and greater flexibility. In contrast, both ligand-bound systems exhibit more compact, distinct clustering within positive PC1 regions, with minimal overlap with the apo system or with each other. This separation of conformational space strongly suggests that ligand binding, whether with Lurtotecan or the control compound, induces a shift in HER2's dynamic behavior toward more restricted and stable states. A 200-ns MD study of HER2 with small-molecule inhibitors showed that ligand-bound systems occupy a distinct low-energy basin, indicating conformational stabilization [76]. The observed clustering implies that both Lurtotecan and the reference ligand constrain the receptor's conformational flexibility and guide the protein into specific low-energy conformational basins. This ligand-induced stabilization of HER2 dynamics reinforces the potential of Lurtotecan as a viable HER2-targeted therapeutic agent by promoting a structurally stable and functionally relevant protein state.

FEL analysis is a critical component of HER2 inhibitor studies, as it enables the identification of the most thermodynamically stable conformational states of the HER2-inhibitor complex. FEL maps protein conformational space using free-energy distributions, highlighting low-energy basins associated with stable structures, effective ligand binding, and protein stability. When integrated with PCA, FEL provides a powerful framework for understanding dynamic transitions and the structural impact of ligand binding on HER2 [76]. ELs of the three simulated systems, apo HER2 (black), the Lurtotecan-HER2 complex (red), and the Control-HER2 complex (green), were projected along the first two principal components (PC1 and PC2) and visualized as contour plots (Figure 4b). The color gradient represents free energy levels, ranging from low (purple) to high (yellow). The FEL of the apo HER2 receptor exhibits two distinct energy minima, suggesting that in the absence of ligand, the protein samples multiple stable conformational states with higher flexibility (Figure 4b). In contrast, the FEL for the Lurtotecan-HER2 complex displays a more confined landscape with a single, well-defined energy minimum, indicating that ligand binding restricts conformational freedom and stabilizes the receptor into a specific low-energy state (Figure 4b). The Control-HER2 complex also shows a distinct energy basin separate from both the apo and Lurtotecan systems, suggesting that the control ligand exerts a distinct yet similarly stabilizing effect on HER2 dynamics (Figure 4b). MD simulations combined with PCA and FEL analysis have demonstrated that potent small-molecule HER2 inhibitors occupy distinct, well-defined low-energy basins, while the apo HER2 receptor maintains broader conformational freedom [5,76].

In HER2-L755S mutant complexes, ibrutinib binding significantly restricted receptor conformational sampling, forming a compact Gibbs free energy basin [78]. Similarly, long-timescale MD simulations of HER2-peptide complexes, such as pep-7, revealed stable binding and well-defined FEL minima, indicating ligand-induced stabilization of constrained conformations [79]. These FEL observations are consistent with the PCA results, reinforcing the conclusion that ligand binding narrows conformational sampling and promotes the adoption of energetically favorable states. The distinct energy landscapes observed for Lurtotecan and the reference compound highlight the ligand-dependent modulation of HER2's structural dynamics, further supporting the potential of Lurtotecan as a promising HER2-targeted therapeutic agent.

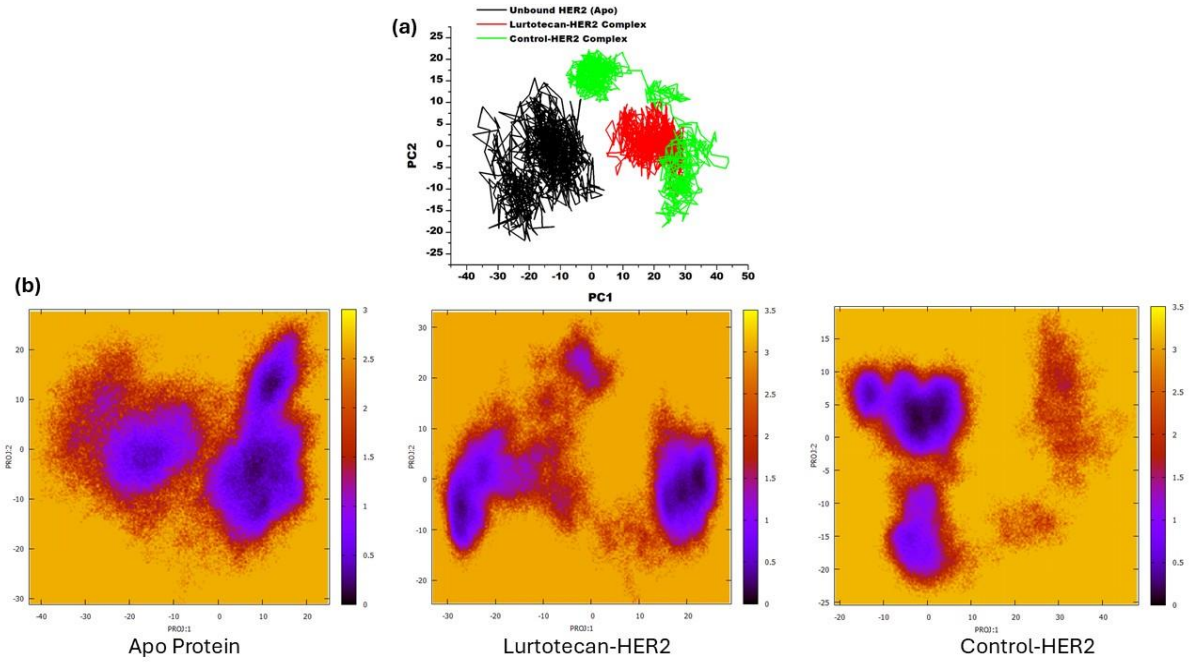


**Figure 4. (a)** Principal component analysis (PCA) of HER2 protein in the apo (unbound) state (black) and in complexes with Lurtotecan (red) and the control ligand (green); **(b)** Corresponding 2D Free energy landscape (FEL) plots, illustrating conformational sampling, low-energy basins, and ligand-induced stabilization of the protein.

*3.4. Binding free energy calculation using MM/GBSA.*

MM/GBSA is a robust post-processing method commonly used to estimate the binding free energy between target proteins and potential inhibitors. MM/GBSA provides deeper thermodynamic insight into ligand-receptor interactions than docking scores alone by decomposing the total binding free energy into distinct contributions, including van der Waals, electrostatic, solvation, and gas-phase energies [80,81]. This technique has proven effective in identifying promising bioactive agents, such as natural compounds from Mangifera indica, that demonstrate superior HER2-binding affinity compared to standard drugs like neratinib [80]. Moreover, MM/GBSA helps reveal the dominant forces driving complex stability and identifies key residues within the binding pocket, thereby facilitating rational drug design and optimization [82].

In this study, MM/GBSA analysis was performed to evaluate the thermodynamic stability and binding strength of HER2-ligand complexes. The binding free energy (ΔGbind) was calculated along with van der Waals energy (ΔEvdw), electrostatic energy (ΔEele), gas-phase energy (ΔGgas), and solvation energy (ΔGsol), expressed in kcal/mol. For the Lurtotecan-HER2 complex, the ΔGbind was -26.13 ± 8.50 kcal/mol, indicating a favorable

binding interaction (Table 3). This interaction was predominantly driven by strong van der Waals forces (ΔEvdw = -38.23 ± 6.82 kcal/mol), implying excellent steric complementarity and hydrophobic engagement with the HER2 binding pocket. Notably, despite an unfavorable electrostatic component (ΔEele = 133.33 ± 38.19 kcal/mol), the complex achieved stability through a significantly favorable solvation energy (ΔGsol = -121.23 ± 35.89 kcal/mol), likely due to polar interactions and HBs with solvent molecules. Consequently, the overall gas-phase energy (ΔGgas = 95.09 ± 40.86 kcal/mol) was effectively counteracted by solvent-mediated stabilization. In comparison, the control compound exhibited a slightly less favorable ΔGbind of -24.18 ± 6.21 kcal/mol, suggesting moderately weaker but still stable binding (Table 3). The control complex showed a more favorable van der Waals contribution (ΔEvdw = -40.12 ± 3.50 kcal/mol), indicating robust hydrophobic interactions. Unlike Lurtotecan, the control ligand displayed favorable electrostatic energy (ΔEele = -19.40 ± 12.31 kcal/mol), which contributed to an overall beneficial gas-phase energy (ΔGgas = -59.53 ± 13.33 kcal/mol). However, this was offset by an unfavorable solvation energy (ΔGsol = 35.34 ± 8.50 kcal/mol), potentially due to desolvation penalties or weaker water-mediated stabilization (Table 3). An MM/GBSA study of novel isoxazole-substituted HER2 inhibitors showed that van der Waals and nonpolar contributions were the main stabilizing forces. In contrast, electrostatic and polar solvation terms were less favorable or destabilizing [83]. Similarly, computational screening of natural compounds against HER2 revealed modest ΔGbind values (-11.0 kcal/mol), with hydrophobic interactions dominating and electrostatics contributing variably [5]. In contrast, a designed HER2 inhibitor (DB15187) achieved a highly favorable ΔGbind of -63.60 ± 3.39 kcal/mol, reflecting an optimized balance of gas-phase and solvation effects [63]. Overall, the MM/GBSA analyses reveal contrasting binding mechanisms for the two compounds. Lurtotecan exhibits a favorable binding free energy mainly through solvent-mediated stabilization, whereas the control ligand relies more on gas-phase electrostatic interactions. These differing energy contributions emphasize Lurtotecan's distinctive interaction dynamics and reinforce its potential as a promising HER2-targeted therapeutic candidate.

**Table 3.** Comparative binding free energy (MM/GBSA) analysis of Lurtotecan-HER2 and control-HER2 complexes, including contributions from van der Waals, electrostatic, solvation, gas-phase, and solvation interactions.

| System | Energy components | | | | |
|---|---|---|---|---|---|
| | **$\Delta E_{vdw}$ (Kcal/mol)** | **$\Delta E_{ele}$ (Kcal/mol)** | **$\Delta G_{gas}$ (Kcal/mol)** | **$\Delta G_{sol}$ (Kcal/mol)** | **$\Delta G_{bind}$ (Kcal/mol)** |
| Lurtotecan Complex | -38.23±6.82 | 133.33±38.19 | 95.09± 40.86 | -121.23±35.89 | -26.13±8.50 |
| Control Complex | -40.12±3.50 | -19.40±12.31 | -59.53±13.33 | 35.34±8.50 | -24.18±6.21 |

$\Delta E_{VDw}$ =van der Waals energy, $\Delta E_{elec}$=Electrostatic energy, $\Delta E_{gas}$=gas phase free energy, $\Delta G_{sol}$ =solvation free energy and $\Delta G_{bind}$=Total binding free energy.

*3.5. Mechanism of action study.*

3.5.1. Network construction, gene ontology (GO), and Kyoto Encyclopedia of genes and genomes (KEGG) pathway enrichment analysis.

A total of 3004 BC-related targets were retrieved from the GeneCards database, of which all were unique targets (Table S1). Additionally, 100 Lurtotecan-related targets were identified in the SwissTargetPrediction database, all of which were unique (Table S2). The intersection of the 3004 BC-related targets and the 100 Lurtotecan-related targets revealed 52 overlapping targets (Figure 5 and Table S3).

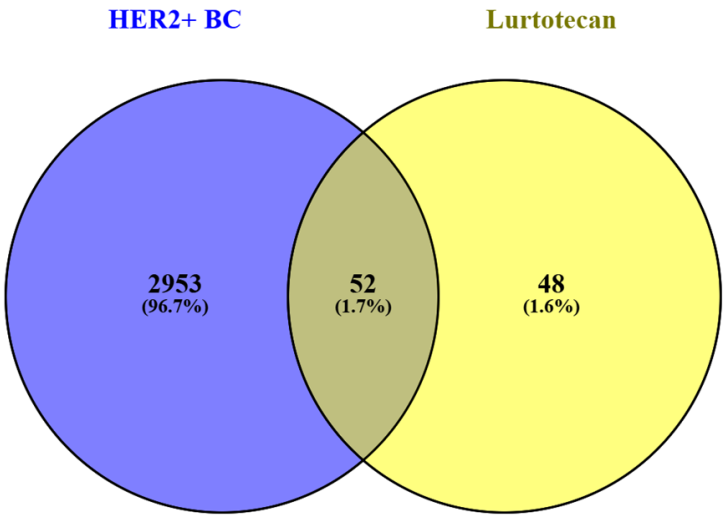


**Figure 5.** Venn diagram showing the core targets shared between Lurtotecan-related targets and BC-related targets, highlighting potential therapeutic intersections for $HER2^{+}$ BC.

To further explore the potential molecular mechanisms of Lurtotecan, a protein-protein interaction (PPI) network was constructed based on the 52 overlapping target genes using the STRING database (Table S4).

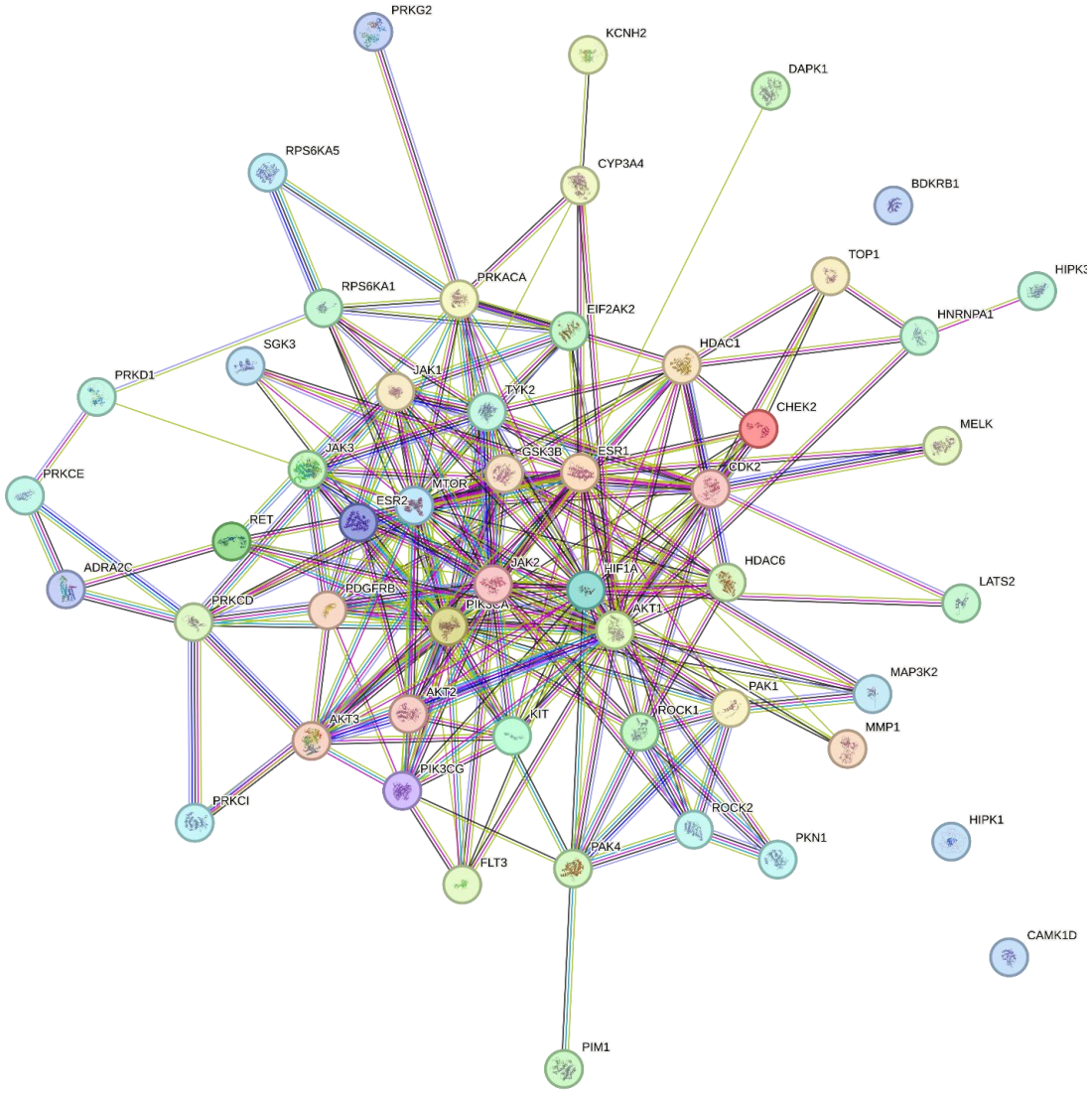


(a)

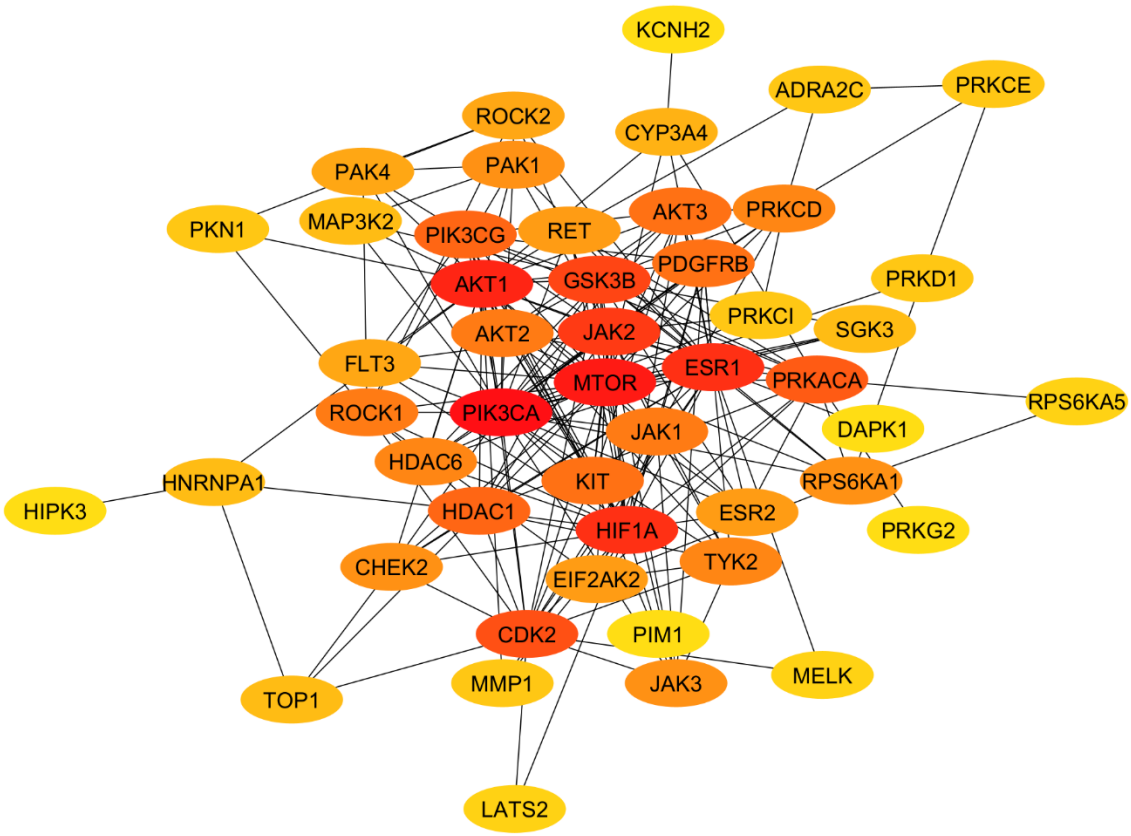


(b)

**Figure 6.** Protein-protein interaction (PPI) analysis of key targets shared between Lurtotecan-related and BC-related targets. **(a)** PPI network generated using STRING software; **(b)** PPI network visualized and analyzed with Cytoscape 3.10.2, highlighting central nodes and interaction strength.

The PPI network was generated by excluding isolated targets and setting the interaction score threshold between connected nodes to >0.613 (Figure 6a). The network consisted of 52 connected nodes and 218 edges, with an average degree value of 8.38. The PPI network was visualized using Cytoscape 3.10.2 software (Figure 6b). Additionally, the node ranks were determined by setting the degree parameter in the CytoHubba plugin in Cytoscape 3.10.2. Furthermore, the 52 overlapping genes were subjected to GO and KEGG analyses using the DAVID software.

We subsequently conducted GO annotation, enrichment analysis, and KEGG pathway mapping for the overlapping targets between Lurtotecan and BC. A total of 52 common genes were analyzed using the DAVID database to obtain GO terms, which were classified into three categories: biological processes (BP), cellular components (CC), and molecular functions (MF) (Figure 7a; Tables S5-S7). The GO analysis identified 241 BP terms, 32 CC terms, and 95 MF terms, with the top 10 entries from each category ($p \leq 0.01$) selected for visualization.

In the BP category, the most significantly enriched processes included protein phosphorylation, chromatin remodeling, intracellular signal transduction, protein autophosphorylation, peptidyl-serine phosphorylation, insulin receptor signaling, positive regulation of the MAPK cascade, activation of the PI3K/AKT pathway, and cytokine-mediated signaling (Figure 7a; Table S5). For CC, the predicted target proteins were predominantly localized in the cytoplasm, cytosol, plasma membrane, nucleoplasm, nucleus, endosome, and receptor complexes, including both intrinsic and extrinsic components of the plasma membrane (Figure 7a; Table S6). In the MF category, the enriched terms were mainly associated with

protein serine/threonine kinase activity, ATP binding, histone kinase activity (e.g., H3T11, H2BS14, H3T3, H2AT120, H2AXS139), and 3-phosphoinositide-dependent protein kinase activity (Figure 7a; Table S7).

Furthermore, KEGG pathway enrichment analysis was performed (Figure 7b; Table S8), and the top 15 pathways with $p \leq 0.01$ were visualized. The most enriched pathways included cancer-related signaling (e.g., PI3K-Akt signaling, central carbon metabolism in cancer, proteoglycans in cancer), viral infection pathways (Kaposi sarcoma-associated herpesvirus, human papillomavirus, and measles), resistance mechanisms (EGFR tyrosine kinase inhibitor resistance), as well as JAK-STAT, chemokine signaling, platelet activation, thyroid hormone signaling, insulin resistance, prolactin signaling, and acute myeloid leukemia (Table Figure 7b; S8). Among the identified pathways, the majority were cancer-associated, suggesting that Lurtotecan holds potential as an alternative therapeutic candidate for $HER2^+$ BC. Moreover, the hsa05200: Pathways in cancer showed interactions with the highest number of target genes (26), which included RET, GSK3B, ROCK1, ROCK2, FLT3, HDAC1, HIF1A, RPS6KA5, AKT2, AKT3, PIM1, AKT1, BDKRB1, JAK2, PRKACA, JAK3, JAK1, PDGFRB, DAPK1, MMP1, ESR1, MTOR, ESR2, PIK3CA, KIT, and CDK2.

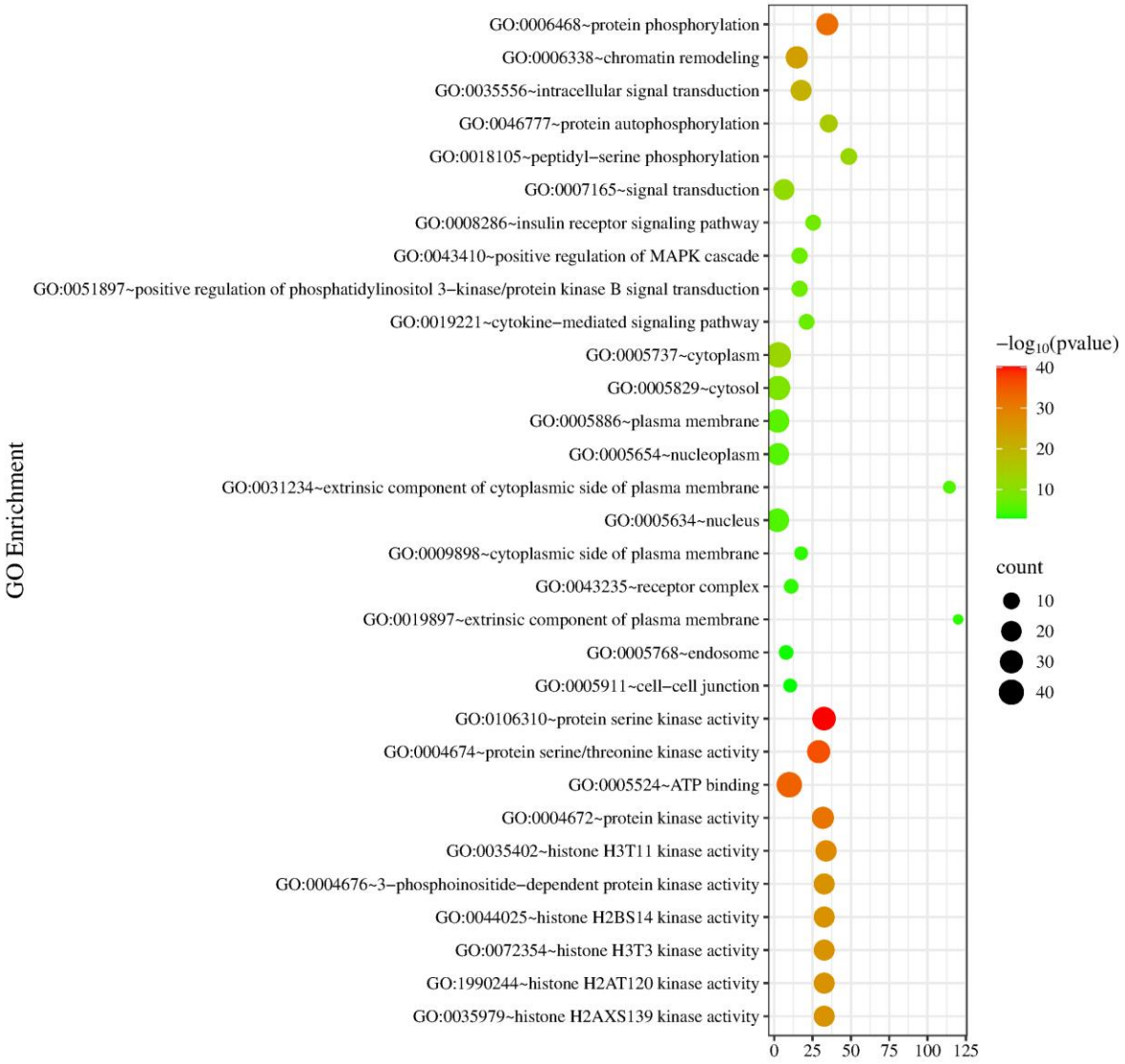


(a)

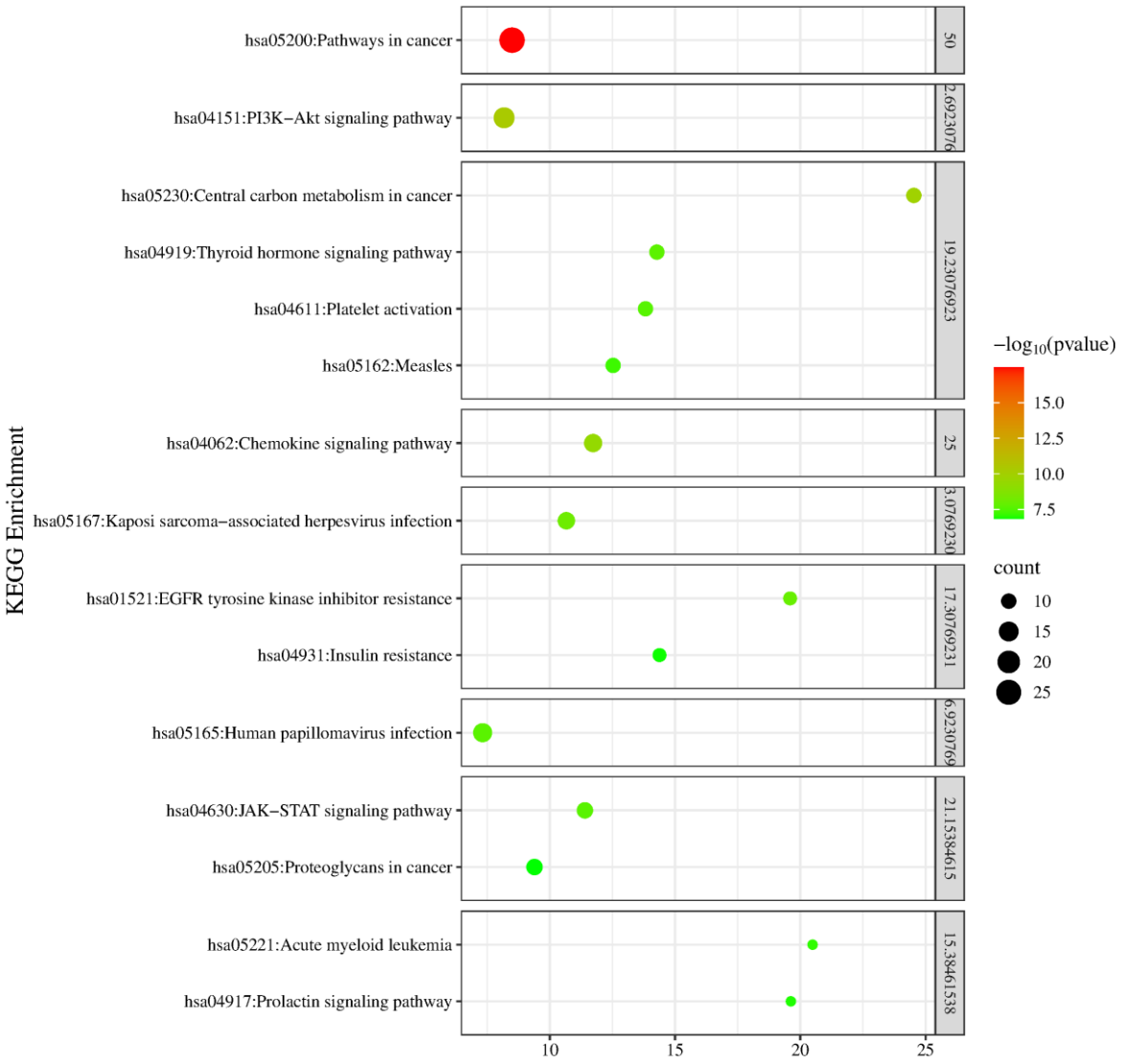


(b)

**Figure 7.** Functional and pathway enrichment analyses of Lurtotecan-related and BC-related targets. **(a)** GO enrichment analysis showing biological processes, molecular functions, and cellular components; **(b)** KEGG pathway enrichment analysis highlighting key signaling pathways potentially modulated by Lurtotecan in BC.

The KEGG pathway hsa05200, "Pathways in cancer," provides a broad framework encompassing multiple signaling routes commonly dysregulated in tumorigenesis, including PI3K-AKT, MAPK, Wnt, p53, apoptosis, and cell cycle regulation [84]. This pathway has been reported as one of the most significantly enriched networks in triple-negative BC (TNBC), with 32 differentially expressed genes identified within hsa05200 ($p = 3.04 \times 10^{\wedge}-25$) and associated subnetworks showing strong enrichment with 19-21 genes ($p = 10^{-13}$ to $10^{-15}$) [85]. Both TNBC and broader BC studies indicate that hsa05200 is frequently highlighted in KEGG-based enrichment analyses of dysregulated genes and in drug-target interaction mapping, suggesting its relevance in therapeutic research [86]. The pathway integrates key oncogenic regulators, including PIK3CA, EGFR, ERBB2 (HER2), and MTOR, making it a useful resource for exploring molecular targets, understanding potential pathway crosstalk, and prioritizing candidate compounds. Accordingly, hsa05200 provides a strategic framework for network pharmacology and drug repurposing approaches to identify potential inhibitors of BC, without implying direct mechanistic causation [84,87].

## 4. Conclusions

This study demonstrates that drug repurposing guided by an integrated *in-silico* framework can serve as a useful and cost-effective strategy for identifying potential candidate molecules targeting $HER2^+$ BC. Through pharmacophore-based virtual screening, molecular docking, binding free-energy estimation, and molecular dynamics simulations, Lurtotecan was identified as a compound capable of forming stable interactions with the HER2 receptor and exhibiting favorable predicted binding energetics. However, these findings are derived from computational analyses and should be considered preliminary predictions rather than confirmed therapeutic activity. Although Trastuzumab Deruxtecan was included as a reference compound during the computational analysis, it belongs to a fundamentally different molecular class and mechanism of action. Therefore, the present results should not be interpreted as evidence of comparable therapeutic efficacy, but rather as an indication that Lurtotecan may interact favorably with the HER2-binding region under simulated conditions. Overall, this study highlights the potential of systematic computational workflows to prioritize candidate molecules and support early-stage drug discovery efforts. Nevertheless, experimental validation remains essential to determine the biological relevance of these predictions. Future investigations should therefore include *in vitro* HER2 inhibition assays, cellular studies in $HER2^+$ BC models, and subsequent *in vivo* evaluations to determine whether the predicted interactions translate into measurable pharmacological effects.

## Author Contributions

Conceptualization, R.M. and M.F.F.M.A.; methodology, R.M. and S.M.I.H; software, A.R.I.; validation, M.F.F.M.A., N.A.B.O., R.M., and A.W.; formal analysis, S.M.I.H.; investigation, R.M.; resources, R.M. and M.F.F.M.A.; data curation, S.M.I.H. and R.M.; writing—original draft preparation, S.M.I.H. and R.M.; writing—review and editing, K.N.C., S.D., N.A.B.O., J.S., M.F.F.M.A.; visualization, S.M.I.H. and R.M.; supervision, M.F.F.M.A.; project administration, M.F.F.M.A.; funding acquisition, M.F.F.M.A. All authors have read and agreed to the published version of the manuscript.

## Institutional Review Board Statement

Not applicable.

## Informed Consent Statement

Not applicable.

## Data Availability Statement

Data can be available upon request.

## Funding

The authors would like to thank Universiti Malaysia Pahang Al-Sultan Abdullah for providing financial support under grant number RDU242749, and Universitas Muhammadiyah Riau for providing financial support under grant number UIC241552.

## Acknowledgments

The authors would like to thank the Faculty of Industrial Sciences and Technology, Universiti Malaysia Pahang, Al-Sultan Abdullah, Malaysia.

## Conflicts of Interest

The authors declare no conflict of interest.

## Role of Funders

The authors would like to thank Universiti Malaysia Pahang Al-Sultan Abdullah for providing financial support under grant number RDU242749, and Universitas Muhammadiyah Riau for providing financial support under grant number UIC241552.

## Supplementary Information

**Table S1.** Breast cancer-related 3004 targets retrieved from the GeneCard database associated with BC.
**Table S2.** Lurtotecan-related 100 targets retrieved from the SwissTargetPrediction database.
**Table S3.** 52 overlapping targets from Venny software using 3004 targets associated with BC and 100 targets associated with Lurtotecan.
**Table S4.** Protein-Protein Interaction (PPI) using 52 overlapping targets from the STRING database.
**Table S5.** 241 Biological Process (BP) data of Gene Ontology (GO).
**Table S6.** 32 Cellular Component (CC) data of Gene Ontology (GO).
**Table S7.** 95 Molecular Function (MF) data of Gene Ontology (GO).
**Table S8.** 121 KEGG signaling pathway.

Download link

## Abbreviations

The following abbreviations are used in this manuscript:

| Abbreviation | Definition |
|---|---|
| HER2 | Human Epidermal Growth Factor Receptor 2 |
| BC | Breast Cancer |
| MD | Molecular Dynamics |
| RMSD | Root Mean Square Deviation |
| RMSF | Root Mean Square Fluctuations |
| RoG | Radius of Gyration |
| HB | Hydrogen Bonding |
| HBs | Hydrogen Bonds |
| ADCs | Antibody-drug Conjugates |
| SMILES | Simplified Molecular Input Line Entry System |
| GO | Gene Ontology |
| KEGG | Kyoto Encyclopedia of Genes and Genomes |
| BP | Biological Processes |
| CC | Cellular Components |
| MF | Molecular Functions |
| PPI | Protein-protein Interaction |
| PCA | Principal Component Analysis |
| FEL | Free-energy Landscape |

## References

1. Cao, W.; Qin, K.; Li, F.; Chen, W. Comparative study of cancer profiles between 2020 and 2022 using global cancer statistics (GLOBOCAN). *J. Natl. Cancer Cent.* **2024**, *4*, 128-134, https://doi.org/10.1016/j.jncc.2024.05.001.

2. Lamichhane, S.; Rai, R.P.; Khatri, A.; Adhikari, R.; Shrestha, B.G.; Shrestha, S.K. Screening of phytochemicals as potential anti-breast cancer agents targeting HER2: an in-silico approach. *J. Biomol. Struct. Dyn.* **2023**, *41*, 897-911, https://doi.org/10.1080/07391102.2021.2014972.
3. Christina, Y.I.; Nafisah, W.; Atho'illah, M.F.; Rifa'i, M.; Widodo, N.; Djati, M.S. Anti-breast cancer potential activity of *Phaleria macrocarpa* (Scheff.) Boerl.leaf extract through *in silico*. *J. Pharm. Pharmacogn. Res.* **2021**, *9*, 824–845, https://doi.org/10.56499/jppres21.1092_9.6.824.
4. Hossam, A.; Abdallah, I.I.; El-Sebakhy, N.A.; Alnajjar, R.; Mohyeldin, M.M. Discovery of natural scaffolds as HER2 inhibitors for breast cancer: virtual screening, molecular dynamics, and biological characterization with selectivity profiling. *Sci. Rep.* **2025**, *15*, 25883, https://doi.org/10.1038/s41598-025-11177-6.
5. Sohrab, S.S.; Kamal, M.A. Screening, Docking, and Molecular Dynamics Study of Natural Compounds as an Anti-HER2 for the Management of Breast Cancer. *Life* **2022**, *12*, 1729, https://doi.org/10.3390/life12111729.
6. Modi, S.; Saura, C.; Yamashita, T.; Park Yeon, H.; Kim, S.-B.; Tamura, K.; Andre, F.; Iwata, H.; Ito, Y.; Tsurutani, J.; Sohn, J.; Denduluri, N.; Perrin, C.; Aogi, K.; Tokunaga, E.; Im, S.-A.; Lee Keun, S.; Hurvitz Sara, A.; Cortes, J.; Lee, C.; Chen, S.; Zhang, L.; Shahidi, J.; Yver, A.; Krop, I. Trastuzumab Deruxtecan in Previously Treated HER2-Positive Breast Cancer. *N. Engl. J. Med.* **2020**, *382*, 610-621, https://doi.org/10.1056/NEJMoa1914510.
7. Cortés, J.; Kim, S.-B.; Chung, W.-P.; Im, S.-A.; Park Yeon, H.; Hegg, R.; Kim Min, H.; Tseng, L.-M.; Petry, V.; Chung, C.-F.; Iwata, H.; Hamilton, E.; Curigliano, G.; Xu, B.; Huang, C.-S.; Kim Jee, H.; Chiu Joanne, W.Y.; Pedrini Jose, L.; Lee, C.; Liu, Y.; Cathcart, J.; Bako, E.; Verma, S.; Hurvitz Sara, A. Trastuzumab Deruxtecan versus Trastuzumab Emtansine for Breast Cancer. *N. Engl. J. Med.* **2022**, *386*, 1143-1154, https://doi.org/10.1056/NEJMoa2115022.
8. Hajdu, S.I.; Darvishian, F. A note from history: Landmarks in history of cancer, part 5. *Cancer* **2013**, *119*, 1450–1466, https://doi.org/10.1002/cncr.27889.
9. Holohan, C.; Van Schaeybroeck, S.; Longley, D.B.; Johnston, P.G. Cancer drug resistance: an evolving paradigm. *Nat. Rev. Cancer* **2013**, *13*, 714-726, https://doi.org/10.1038/nrc3599.
10. Pushpakom, S.; Iorio, F.; Eyers, P.A.; Escott, K.J.; Hopper, S.; Wells, A.; Doig, A.; Guilliams, T.; Latimer, J.; McNamee, C.; Norris, A.; Sanseau, P.; Cavalla, D.; Pirmohamed, M. Drug repurposing: progress, challenges and recommendations. *Nat. Rev. Drug Discov.* **2019**, *18*, 41-58, https://doi.org/10.1038/nrd.2018.168.
11. Zoete, V.; Daina, A.; Bovigny, C.; Michielin, O. SwissSimilarity: A Web Tool for Low to Ultra High Throughput Ligand-Based Virtual Screening. *J. Chem. Inf. Model.* **2016**, *56*, 1399-1404, https://doi.org/10.1021/acs.jcim.6b00174.
12. Roney, M.; Huq, A.M.; Aluwi, M.F.F.M.; Tajuddin, S.N. *In-silico* Design of Curcumin Analogs as Potential Inhibitors of Dengue Virus NS2B/NS3 Protease. *J. Comput. Biophys. Chem.* **2023**, *22*, 645–653, https://doi.org/10.1142/S2737416523500321.
13. Modi, S.; Jacot, W.; Yamashita, T.; Sohn, J.; Vidal, M.; Tokunaga, E.; Tsurutani, J.; Ueno Naoto, T.; Prat, A.; Chae Yee, S.; Lee Keun, S.; Niikura, N.; Park Yeon, H.; Xu, B.; Wang, X.; Gil-Gil, M.; Li, W.; Pierga, J.-Y.; Im, S.-A.; Moore Halle, C.F.; Rugo Hope, S.; Yerushalmi, R.; Zagouri, F.; Gombos, A.; Kim, S.-B.; Liu, Q.; Luo, T.; Saura, C.; Schmid, P.; Sun, T.; Gambhire, D.; Yung, L.; Wang, Y.; Singh, J.; Vitazka, P.; Meinhardt, G.; Harbeck, N.; Cameron David, A. Trastuzumab Deruxtecan in Previously Treated HER2-Low Advanced Breast Cancer. *N. Engl. J. Med.* **2022**, *387*, 9-20, https://doi.org/10.1056/NEJMoa2203690.
14. Oliveira, T.A.d.; Silva, M.P.d.; Maia, E.H.B.; Silva, A.M.d.; Taranto, A.G. Virtual Screening Algorithms in Drug Discovery: A Review Focused on Machine and Deep Learning Methods. *Drugs Drug Candidates* **2023**, *2*, 311-334, https://doi.org/10.3390/ddc2020017.
15. Du, J.; Sun, H.; Xi, L.; Li, J.; Yang, Y.; Liu, H.; Yao, X. Molecular modeling study of checkpoint kinase 1 inhibitors by multiple docking strategies and prime/MM–GBSA calculation. *J. Comput. Chem.* **2011**, *32*, 2800-2809, https://doi.org/10.1002/jcc.21859.
16. Nyambo, K.; Tapfuma, K.I.; Adu-Amankwaah, F.; Julius, L.; Baatjies, L.; Niang, I.S.; Smith, L.; Govender, K.K.; Ngxande, M.; Watson, D.J.; Wiesner, L.; Mavumengwana, V. Molecular docking, molecular dynamics simulations and binding free energy studies of interactions between *Mycobacterium tuberculosis* Pks13, PknG and bioactive constituents of extremophilic bacteria. *Sci. Rep.* **2024**, *14*, 6794, https://doi.org/10.1038/s41598-024-57124-9.
17. Abbasi, M.; Mansourian, M.; Oskouie, A.A.; Taheri, S.; Mahnam, K. *In-silico* study MM/GBSA binding free energy and molecular dynamics simulation of some designed remdesivir derivatives as the inhibitory

potential of SARS-CoV-2 main protease. *Res. Pharma. Sci.* **2024**, *19*, 29–41, https://doi.org/10.4103/1735-5362.394818.

18. Tsurutani, J.; Iwata, H.; Krop, I.; Jänne, P.A.; Doi, T.; Takahashi, S.; Park, H.; Redfern, C.; Tamura, K.; Wise-Draper, T.M.; Saito, K.; Sugihara, M.; Singh, J.; Jikoh, T.; Gallant, G.; Li, B.T. Targeting HER2 with Trastuzumab Deruxtecan: A Dose-Expansion, Phase I Study in Multiple Advanced Solid Tumors. *Cancer Discov.* **2020**, *10*, 688-701, https://doi.org/10.1158/2159-8290.CD-19-1014.
19. Seiden, M.V.; Muggia, F.; Astrow, A.; Matulonis, U.; Campos, S.; Roche, M.; Sivret, J.; Rusk, J.; Barrett, E. A phase II study of liposomal lurtotecan (OSI-211) in patients with topotecan resistant ovarian cancer. *J. Gynecol. Oncol.* **2004**, *93*, 229-232, https://doi.org/10.1016/j.ygyno.2003.12.037.
20. Haglof, K.J.; Popa, E.; Hochster, H.S. Recent developments in the clinical activity of topoisomerase-1 inhibitors. *Update Cancer Ther.* **2006**, *1*, 117-145, https://doi.org/10.1016/j.uct.2006.05.010.
21. Anighoro, A.; Bajorath, J.; Rastelli, G. Polypharmacology: Challenges and Opportunities in Drug Discovery. *J. Med. Chem.* **2014**, *57*, 7874–7887, https://doi.org/10.1021/jm5006463.
22. Schaefer, G.; Shao, L.; Totpal, K.; Akita, R.W. Erlotinib Directly Inhibits HER2 Kinase Activation and Downstream Signaling Events in Intact Cells Lacking Epidermal Growth Factor Receptor Expression. *Cancer Res.* **2007**, *67*, 1228–1238, https://doi.org/10.1158/0008-5472.CAN-06-3493.
23. Hamim, S.M.I.; Uddin, M.N.; Roney, M.; Chhando, K.S.; Birang, A.B.; Yelansaran, M.V.; Aluwi, M.F.F.M.; Omar, N.A.M. Exploring the Wound Healing Efficacy of Kyllinga nemoralis: Phytochemical Analysis, Network Pharmacology, Molecular Docking, and Molecular Dynamics Simulations. *J. Pharm. Innov.* **2026**, *21*, 196, https://doi.org/10.1007/s12247-026-10435-y.
24. Hamim, S.M.I.; Roney, M.; Uddin, M.N.; Issahaku, A.R.; Chhando, K.S.; Aluwi, M.F.F.M.; Omar, N.A.M. Investigating the potential compounds of *Kalanchoe pinnata* plant for the treatment of inflammation utilizing molecular docking and molecular dynamic simulation approach. *In silico Res. Biomed.* **2025**, *1*, 100007, https://doi.org/10.1016/j.insi.2025.100007.
25. Alamri, M.A.; Alamri, M.A. Pharmacophore and docking-based sequential virtual screening for the identification of novel Sigma 1 receptor ligands. *Bioinformation* **2019**, *15*, 586–595, https://doi.org/10.6026/97320630015586.
26. Wilding, B.; Scharn, D.; Böse, D.; Baum, A.; Santoro, V.; Chetta, P.; Schnitzer, R.; Botesteanu, D.A.; Reiser, C.; Kornigg, S.; Knesl, P.; Hörmann, A.; Köferle, A.; Corcokovic, M.; Lieb, S.; Scholz, G.; Bruchhaus, J.; Spina, M.; Balla, J.; Peric-Simov, B.; Zimmer, J.; Mitzner, S.; Fett, T.N.; Beran, A.; Lamarre, L.; Gerstberger, T.; Gerlach, D.; Bauer, M.; Bergner, A.; Schlattl, A.; Bader, G.; Treu, M.; Engelhardt, H.; Zahn, S.; Fuchs, J.E.; Zuber, J.; Ettmayer, P.; Pearson, M.; Petronczki, M.; Kraut, N.; McConnell, D.B.; Solca, F.; Neumüller, R.A. Discovery of potent and selective HER2 inhibitors with efficacy against HER2 exon 20 insertion-driven tumors, which preserve wild-type EGFR signaling. *Nat. Cancer* **2022**, *3*, 821-836, https://doi.org/10.1038/s43018-022-00412-y.
27. Molla, M.H.R.; Asseri, A.H.; Islam, Md.S. Integrated structure model-based virtual screening approaches identified anti-cancer agents against prostate cancer by targeting MAOB protein. *Egypt J. Med. Hum. Genet.* **2023**, *24*, 51, https://doi.org/10.1186/s43042-023-00431-z.
28. Prabhavathi, H.; Dasegowda, K.R.; Renukananda, K.H.; Karunakar, P.; Lingaraju, K.; Raja Naika, H. Molecular docking and dynamic simulation to identify potential phytocompound inhibitors for EGFR and HER2 as anti-breast cancer agents. *J. Biomol. Struct. Dyn.* **2022**, *40*, 4713-4724, https://doi.org/10.1080/07391102.2020.1861982.
29. Roney, M.; Mohd Hisam, N.S.; Uddin, M.N.; Istiaque Hamim, S.M.; Lim, L.W.; Wong, K.H. Repurposing of natural products for spinocerebellar ataxia type 3 using integrated network pharmacology and *in silico* approaches. *Sci. Rep.* **2026**, *16*, 7332, https://doi.org/10.1038/s41598-025-30652-8.
30. Agarwal, R.; Smith, J.C. Speed vs Accuracy: Effect on Ligand Pose Accuracy of Varying Box Size and Exhaustiveness in AutoDock Vina. *Mol. Inform.* **2023**, 42, 2200188, https://doi.org/10.1002/minf.202200188.
31. Varakumar, P.; Rajagopal, K.; Islam, F.; Raman, K.; Byran, G.; Gurunathan, M.; Prema, S.; Murugesan, T.; Chitrapu, P.; Barua, R. Identifying Potent 9-Anilinoacridine-Based HER2 Breast Cancer Inhibitors Using *in silico* Computational Approaches. *J. Biol. Regul. Homeost. Agents* **2023**, 37, 6511-6523, https://doi.org/10.23812/j.biol.regul.homeost.agents.20233712.616.
32. Roney, M.; Issahaku, A.R.; Dubey, A.; Tufail, A.; Istiaque Hamim, S.M.; Wilhelm, A.; Aluwi, M.F.F.M. In-silico evaluation of diffractaic acid as novel anti-diabetic inhibitor against dipeptidyl peptidase IV enzyme. *In silico Pharmacol.* **2025**, *13*, 24, https://doi.org/10.1007/s40203-025-00321-9.

33. Thuluz, M.-M.; Marcela, L.-S.; Angel, T.; Rossana, C.Z.; Manuel, E.M.; Rodrigo, G.-M. Elucidating Molecular Interactions of Ten Natural Compounds Targeting E6 HPV High Risk Oncoproteins Using Microsecond Molecular Dynamics Simulations. *Med. Chem.* **2021**, *17*, 587–600, https://doi.org/10.2174/1573406416666200129145733.
34. Mariana Kustiawan, P.; Siregar, K.A.A.K.; Syaifie, P.H.; Zein Muttaqin, F.; Ibadillah, D.; Miftah Jauhar, M.; Djamas, N.; Mardliyati, E.; Taufiqu Rochman, N. Uncovering the anti-breast cancer activity potential of east Kalimantan propolis by In vitro and bioinformatics analysis. *Heliyon* **2024**, *10*, e33636, https://doi.org/10.1016/j.heliyon.2024.e33636.
35. Anjum, R.; Jain, K.; Meena, K.; Dua, A. *In silico* studies of triazole derivatives as inhibitors for estrogen receptor (ER) mutant L536S and anaplastic lymphoma kinase: DFT/tD-DFT, molecular docking, and MD simulations. *J. Biomol. Struc. Dynam.* **2026**, *44*, 1310–1332, https://doi.org/10.1080/07391102.2024.2434688.
36. Kumari, S.; Sobhia, M.E. Targeting an Old Foe for Cancer: A Molecular Dynamics Perspective to Unravel the Specific Binding Nature of 2-Methoxy Estradiol to Human β-Tubulin Isotypes. *J. Chem. Inf. Model.* **2024**, 64, 4121–4133, https://doi.org/10.1021/acs.jcim.4c00438.
37. Fang, D.; Zhang, Z.; Zhai, J.; Guo, B.; Li, P.; Liu, X.; Song, J.; Xie, S.; Wu, R.; Zhao, Y.; Wang, C. Enzymatic-related network of catalysis, polyamine, and tumors for acetylpolyamine oxidase: from calculation to experiment. *Chem. Sci.* **2024**, *15*, 2867–2882, https://doi.org/10.1039/D3SC06037C.
38. Zheng, G.; Liu, W.; Zhang, Q.; Shen, T.; Zhang, J.; Jiang, L.; Liang, W.; Zhou, B.; Liu, L.; Xu, S.; Li, M. Molecular docking and molecular dynamics simulations reveal the clinical resistance of the gatekeeper mutation V564F of FGFR2 against Infigratinib. *J. Exp. Nanosci.* **2023**, *18*, 2264521, https://doi.org/10.1080/17458080.2023.2264521.
39. Mahapatra, S.; Kar, P. Identification and characterization of binding thermodynamics and kinetics of inhibitors targeting FGFR1 *via* molecular modelling and ligand Gaussian accelerated molecular dynamics simulations. *Phys. Chem. Chem. Phys.* **2025**, *27*, 10137–10152, https://doi.org/10.1039/D4CP04690K.
40. Cvijetić, I.N.; Herlah, B.; Marinković, A.; Perdih, A.; Bjelogrlić, S.K. Phenotypic Discovery of Thiocarbohydrazone with Anticancer Properties and Catalytic Inhibition of Human DNA Topoisomerase IIα. *Pharmaceuticals* **2023**, *16*, 341, https://doi.org/10.3390/ph16030341.
41. Issahaku, A.R.; Mncube, S.M.; Agoni, C.; Kwofie, S.K.; Alahmdi, M.I.; Abo-Dya, N.E.; Sidhom, P.A.; Tawfeek, A.M.; Ibrahim, M.A.A.; Mukelabai, N.; Soremekun, O.; Soliman, M.E.S. Multi-dimensional structural footprint identification for the design of potential scaffolds targeting METTL3 in cancer treatment from natural compounds. *J. Mol. Model.* **2023**, *29*, 122, https://doi.org/10.1007/s00894-023-05516-5.
42. Hu, H.; Chen, B.; Zheng, D.; Huang, G. Revealing the selective mechanisms of inhibitors to PARP-1 and PARP-2 via multiple computational methods. *PeerJ* **2020**, *8*, e9241, https://doi.org/10.7717/peerj.9241.
43. Maisuradze, G.G.; Liwo, A.; Scheraga, H.A. Principal Component Analysis for Protein Folding Dynamics. *J. Mol. Biol.* **2009**, *385*, 312–329, https://doi.org/10.1016/j.jmb.2008.10.018.
44. Ghufran, M.; Ullah, M.; Khan, H.A.; Ghufran, S.; Ayaz, M.; Siddiq, M.; Abbas, S.Q.; Hassan, S.S.u.; Bungau, S. In-Silico Lead Druggable Compounds Identification against SARS COVID-19 Main Protease Target from In-House, Chembridge and Zinc Databases by Structure-Based Virtual Screening, Molecular Docking and Molecular Dynamics Simulations. *Bioengineering* **2023**, *10*, 100, https://doi.org/10.3390/bioengineering10010100.
45. Zhao, Z.; Zhu, Y.; Long, F.; Ma, Y.; Tang, Q.; Wang, T. Exploring the potential of Huangqin Tang in breast cancer treatment using network pharmacological analysis and experimental verification. *BMC Complement. Med. Ther.* **2024**, *24*, 221, https://doi.org/10.1186/s12906-024-04523-0.
46. Qayoom, H.; Alkhanani, M.; Almilaibary, A.; Alsagaby, S.A.; Mir, M.A. A network pharmacology-based investigation of brugine reveals its multi-target molecular mechanism against Breast Cancer. *Med. Oncol.* **2023**, *40*, 202, https://doi.org/10.1007/s12032-023-02067-w.
47. Wan, X.; Cui, L.; Xiao, Q. Metabolomics and network pharmacology-based identification of phenolic acids in *Polygonatum kingianum* var. *grandifolium* rhizomes as anti-cancer/Tumor active ingredients. *PLOS ONE* **2024**, *19*, e0315857, https://doi.org/10.1371/journal.pone.0315857.
48. Zhang, X.; Shen, T.; Zhou, X.; Tang, X.; Gao, R.; Xu, L.; Wang, L.; Zhou, Z.; Lin, J.; Hu, Y. Network pharmacology based virtual screening of active constituents of *Prunella vulgaris* L. and the molecular mechanism against breast cancer. *Sci. Rep.* **2020**, *10*, 15730, https://doi.org/10.1038/s41598-020-72797-8.

49. Kurmi, S.P.C.; Karati, D. Molecular Targets and Mechanisms of Piperine Against Breast Cancer: A Network Pharmacology, Molecular Docking Analysis, and Toxicity Prediction. *Chem. Biodiver.* **2025**, *22*, e03180, https://doi.org/10.1002/cbdv.202403180.
50. Yang, L.-n.; Wu, Z.-l.; Yang, Z.-j.; Li, S.-g.; Ouyang, C.-s. Exploring Mechanism of Key Chinese Herbal Medicine on Breast Cancer by Data Mining and Network Pharmacology Methods. *Chin. J. Integr. Med.* **2021**, *27*, 919-926, https://doi.org/10.1007/s11655-020-3422-y.
51. Roney, M.; Issahaku, A.R.; Hamim, S.M.I.; Wilhelm, A.; Mohd Aluwi, M.F.F. Repurposing Sulfonamide-Based Antidiabetic Agents Against Polycystic Ovary Syndrome: A Molecular Docking and Dynamics Simulation Approach. *J. Pharm. Innov.* **2025**, *20*, 202, https://doi.org/10.1007/s12247-025-10119-z.
52. Yalaza, C.; Antmen, S.E.; Acuner, S.E.; Oz, H.; Bulut, E.; Canacankatan, N. Identification of novel HER2 ınhibitors: potential therapeutics for breast cancer. *Discov. Oncol.* **2025**, *16*, 1122, https://doi.org/10.1007/s12672-025-02792-w.
53. Sait, K.H.W.; Mashraqi, M.; Khogeer, A.A.; Alzahrani, O.; Anfinan, N.M.; Sait, H.K.; Almutairi, A.; Alam, Q. Molecular docking analysis of HER-2 inhibitor from the ZINC database as anticancer agents. *Bioinformation* **2020**, *16*, 882, https://doi.org/10.6026/97320630016882.
54. Tang, J.-Y.; Ho, Y.; Chang, C.-Y.; Liu, H.-L. Discovery of Novel Irreversible HER2 Inhibitors for Breast Cancer Treatment. *J. Biomed. Sci. Eng.* **2019**, *12*, 225, https://doi.org/10.4236/jbise.2019.124016.
55. Almasoudi, H.H.; Mashraqi, M.M.; Alshamrani, S.A.; Alharthi, A.A.; Alsalmi, O.; Nahari, M.H.; Al-Mansour, F.S.H.; Alhazmi, A.Y.M. Structure-Based *In silico* Approaches Reveal IRESSA as a Multitargeted Breast Cancer Regulatory, Signalling, and Receptor Protein Inhibitor. *Pharmaceuticals* **2024**, *17*, 208, https://doi.org/10.3390/ph17020208.
56. Akinnusi, P.A.; Olubode, S.O.; Adebesin, A.O.; Nana, T.A.; Shodehinde, S.A. Discovery of promising inhibitors of epidermal growth factor receptor (EGFR), human epidermal growth factor receptor 2 (HER2), estrogen receptor (ER), and phosphatidylinositol-3-kinase a (PI3Ka) for personalized breast cancer treatment. *Cancer Inform*. **2022**, *21*, 11769351221127862, https://doi.org/10.1177/11769351221127862.
57. Sadek, M.M.; Serrya, R.A.; Kafafy, A.-H.N.; Ahmed, M.; Wang, F.; Abouzid, K.A.M. Discovery of new HER2/EGFR dual kinase inhibitors based on the anilinoquinazoline scaffold as potential anti-cancer agents. *J. Enzyme Inhib. Med. Chem.* **2014**, *29*, 215–222, https://doi.org/10.3109/14756366.2013.765417.
58. Warren, G.L.; Andrews, C.W.; Capelli, A.-M.; Clarke, B.; LaLonde, J.; Lambert, M.H.; Lindvall, M.; Nevins, N.; Semus, S.F.; Senger, S.; Tedesco, G.; Wall, I.D.; Woolven, J.M.; Peishoff, C.E.; Head, M.S. A Critical Assessment of Docking Programs and Scoring Functions. *J. Med. Chem.* **2006**, *49*, 5912–5931, https://doi.org/10.1021/jm050362n.
59. Homeyer, N.; Gohlke, H. Free Energy Calculations by the Molecular Mechanics Poisson−Boltzmann Surface Area Method. *Mol. Inform.* **2012**, *31*, 114–122, https://doi.org/10.1002/minf.201100135.
60. Kollman, P.A.; Massova, I.; Reyes, C.; Kuhn, B.; Huo, S.; Chong, L.; Lee, M.; Lee, T.; Duan, Y.; Wang, W.; Donini, O.; Cieplak, P.; Srinivasan, J.; Case, D.A.; Cheatham, T.E. Calculating Structures and Free Energies of Complex Molecules: Combining Molecular Mechanics and Continuum Models. *Acc. Chem. Res.* **2000**, *33*, 889–897, https://doi.org/10.1021/ar000033j.
61. Moukharskaya, J.; Verschraegen, C. Topoisomerase 1 Inhibitors and Cancer Therapy. *Hematol. Oncol. Clin. North Am.* **2012**, *26*, 507-525, https://doi.org/10.1016/j.hoc.2012.03.002.
62. Yadav, M.; Dhagat, S.; Eswari, J.S. Structure Based Drug Design and Molecular Docking Studies of Anticancer Molecules Paclitaxel, Etoposide and Topotecan using Novel Ligands. *Curr. Drug Discov. Technol.* **2020**, *17*, 183–190, https://doi.org/10.2174/1570163816666190307102033.
63. Singh, G.; Al-Fahad, D.; Al-Zrkani, M.K.; Chaudhuri, T.K.; Soni, H.; Tandon, S.; Narasimhaji, C.V.; Azam, F.; Patil, R. Identification of potential inhibitors of HER2 targeting breast cancer—a structure-based drug design approach. *J. Biomol. Struct. Dyn.* **2024**, *42*, 8184-8201, https://doi.org/10.1080/07391102.2023.2246576.
64. Hafez, H.M.; Said, B.A.M.; Sayed, A.M.; Alatwi, E.; Youssif, B.G.M.; Bräse, S.; El-Sherief, H.A.M. Design, synthesis, antiproliferative activity, and molecular dynamics simulation of pyrazoline-based derivatives as dual EGFR and HER-2 inhibitors. *RSC Adv.* **2025**, *15*, 9265–9279, https://doi.org/10.1039/D5RA01169H.
65. Hashmi, A.I.; Iqtedar, M.; Saeed, H.; Ahmed, N.; Abdullah, R.; Kaleem, A.; Abbasi, M.A. Characterization of soil-derived *Bacillus subtilis* metabolites against breast cancer: In vitro and *in silico* studies. *Saudi Pharm. J.* **2025**, *33*, 3, https://doi.org/10.1007/s44446-025-00006-6.

66. Liu, K.; Watanabe, E.; Kokubo, H. Exploring the stability of ligand binding modes to proteins by molecular dynamics simulations. *J. Comput.-Aided Mol. Des.* **2017**, *31*, 201–211, https://doi.org/10.1007/s10822-016-0005-2.
67. Martínez, L. Automatic Identification of Mobile and Rigid Substructures in Molecular Dynamics Simulations and Fractional Structural Fluctuation Analysis. *PLoS ONE* **2015**, *10*, e0119264, https://doi.org/10.1371/journal.pone.0119264.
68. Rahimi, M.; Taghdir, M.; Abasi Joozdani, F. *Dynamozones* are the most obvious sign of the evolution of conformational dynamics in HIV-1 protease. *Sci. Rep.* **2023**, *13*, 14179, https://doi.org/10.1038/s41598-023-40818-x.
69. Saibu, O.A.; Singh, G.; Olugbodi, S.A.; Oluwafemi, A.T.; Ajayi, T.M.; Hammed, S.O.; Oladipo, O.O.; Odunitan, T.T.; Omoboyowa, D.A. Identification of HER2 inhibitors from curcumin derivatives using combination of *in silico* screening and molecular dynamics simulation. *J. Biomol. Struct. Dynam.* **2023**, *41*, 12328–12337, https://doi.org/10.1080/07391102.2023.2175260.
70. Telesco, S.E.; Radhakrishnan, R. Atomistic Insights into Regulatory Mechanisms of the HER2 Tyrosine Kinase Domain: A Molecular Dynamics Study. *Biophys. J.* **2009**, *96*, 2321–2334, https://doi.org/10.1016/j.bpj.2008.12.3912.
71. Oyewusi, H.A.; Wahab, R.A.; Akinyede, K.A.; Albadrani, G.M.; Al-Ghadi, M.Q.; Abdel-Daim, M.M.; Ajiboye, B.O.; Huyop, F. Bioinformatics analysis and molecular dynamics simulations of azoreductases (AzrBmH2) from *Bacillus megaterium* H2 for the decolorization of commercial dyes. *Environ. Sci. Eur.* **2024**, *36*, 31, https://doi.org/10.1186/s12302-024-00853-5.
72. Ghahremanian, S.; Rashidi, M.M.; Raeisi, K.; Toghraie, D. Molecular dynamics simulation approach for discovering potential inhibitors against SARS-CoV-2: A structural review. *J. Mol. Liq.* **2022**, *354*, 118901, https://doi.org/10.1016/j.molliq.2022.118901.
73. Justino, G.C.; Nascimento, C.P.; Justino, M.C. Molecular dynamics simulations and analysis for bioinformatics undergraduate students. *Biochem. Mol. Bio. Educ.* **2021**, *49*, 570–582, https://doi.org/10.1002/bmb.21512.
74. Millan-Casarrubias, E.J.; García-Tejeda, Y.V.; González-De la Rosa, C.H.; Ruiz-Mazón, L.; Hernández-Rodríguez, Y.M.; Cigarroa-Mayorga, O.E. Molecular Docking and Pharmacological *In silico* Evaluation of Camptothecin and Related Ligands as Promising HER2-Targeted Therapies for Breast Cancer. *Curr. Issues Mol. Biol.* **2025**, *47*, 193, https://doi.org/10.3390/cimb47030193.
75. Sun, T.-Y.; Wang, Q.; Zhang, J.; Wu, T.; Zhang, F. Trastuzumab-Peptide Interactions: Mechanism and Application in Structure-Based Ligand Design. *Int. J. Mol. Sci.* **2013**, *14*, 16836-16850, https://doi.org/10.3390/ijms140816836.
76. Lata Tripathi, K.; Chaudhary, A.; Alam, A.; Shukla, D.; Bhardwaj, R.; Badoni, H. Molecular insights from structural dynamics of HER2-inhibitor complexes pave the way for new breast cancer drugs. *J. Biomol. Struct. Dynam.* **2026**, *44*, 809–822, https://doi.org/10.1080/07391102.2024.2425835.
77. R. Magalhães, P.; Machuqueiro, M.; G. Almeida, J.; Melo, A.; D. S. Cordeiro, M.N.; Cabo Verde, S.; H. Gümüş, Z.; S. Moreira, I.; D. G. Correia, J.; Melo, R. Dynamical Rearrangement of Human Epidermal Growth Factor Receptor 2 upon Antibody Binding: Effects on the Dimerization. *Biomolecules* **2019**, *9*, 706, https://doi.org/10.3390/biom9110706.
78. Loganathan, T.; Doss, C.G.P. Computational molecular insights into ibrutinib as a potent inhibitor of HER2-L755S mutant in breast cancer: gene expression studies, virtual screening, docking, and molecular dynamics analysis. *Front. Mol. Biosci.* **2025**, *12*, 1510896, https://doi.org/10.3389/fmolb.2025.1510896.
79. Alkhatabi, H.A.; Alatyb, H.N. *In silico* Design of Peptide Inhibitors Targeting HER2 for Lung Cancer Therapy. *Cancers* **2024**, *16*, 3979, https://doi.org/10.3390/cancers16233979.
80. Balogun, T.A.; Iqbal, M.N.; Saibu, O.A.; Akintubosun, M.O.; Lateef, O.M.; Nneka, U.C.; Abdullateef, O.T.; Omoboyowa, D.A. Discovery of potential HER2 inhibitors from *Mangifera indica* for the treatment of HER2-Positive breast cancer: an integrated computational approach. *J. Biomol. Struct. Dynam.* **2022**, *40*, 12772–12784, https://doi.org/10.1080/07391102.2021.1975570.
81. Balbuena-Rebolledo, I.; Padilla-Martínez, I.I.; Rosales-Hernández, M.C.; Bello, M. Repurposing FDA Drug Compounds against Breast Cancer by Targeting EGFR/HER2. *Pharmaceuticals* **2021**, *14*, 791, https://doi.org/10.3390/ph14080791.
82. Alvarado-Lozano, J.E.; Hernández-Valencia, J.A.; Ávila-Avilés, R.D.; Bello, M. Insight into the inhibitory activity of mangiferin and Silybin against HER2 and EGFR using theoretical and experimental approaches. *Sci. Rep.* **2025**, *15*, 8658, https://doi.org/10.1038/s41598-025-93612-2.

83. Rajagopal, K.; Kalusalingam, A.; Bharathidasan, A.R.; Sivaprakash, A.; Shanmugam, K.; Sundaramoorthy, M.; Byran, G. *In silico* Drug Design of Anti-Breast Cancer Agents. *Molecules* **2023**, *28*, 4175, https://doi.org/10.3390/molecules28104175.
84. López-Cortés, A.; Paz-y-Miño, C.; Cabrera-Andrade, A.; Barigye, S.J.; Munteanu, C.R.; González-Díaz, H.; Pazos, A.; Pérez-Castillo, Y.; Tejera, E. Gene prioritization, communality analysis, networking and metabolic integrated pathway to better understand breast cancer pathogenesis. *Sci. Rep.* **2018**, *8*, 16679, https://doi.org/10.1038/s41598-018-35149-1.
85. Peng, C.; Ma, W.; Xia, W.; Zheng, W. Integrated analysis of differentially expressed genes and pathways in triple-negative breast cancer. *Mol. Med. Rep.* **2017**, *15*, 1087–1094, https://doi.org/10.3892/mmr.2017.6101.
86. Yu, L.; Zhao, J.; Gao, L. Predicting Potential Drugs for Breast Cancer based on miRNA and Tissue Specificity. *Int. J. Biol. Sci.* **2018**, *14*, 971–982, https://doi.org/10.7150/ijbs.23350.
87. Shaala, L.A.; Youssef, D.T.A.; Ramadan, M.A.; Khalifa, A.A.; Ibrahim, R.S.; Valeriote, F.; Celik, I.; Dawood, H.M. Molecular mechanisms of phytoconstituents from selected Egyptian plants against non-small cell lung cancer using integrated in vitro network pharmacology and molecular docking approach. *Naunyn-Schmiedeberg's Arch. Pharmacol.* **2025**, *398*, 9061–9082, https://doi.org/10.1007/s00210-025-03834-4.

## Publisher's Note & Disclaimer